First-principles calculations of the electronic structure and spectra of strongly correlated systems: the **LDA**+ *U* method

1997 J. Phys.: Condens. Matter 9 767

(http://iopscience.iop.org/0953-8984/9/4/002)

J. Phys.: Condens. Matter **9** (1997) 767–808. Printed in the UK PII: S0953-8984(97)76603-7

REVIEW ARTICLE

First-principles calculations of the electronic structure and spectra of strongly correlated systems: the LDA + U method

Vladimir I Anisimov†, F Aryasetiawan‡ and A I Lichtenstein§

† Institute of Metal Physics, Ekaterinburg, GSP-170, Russia

‡ Department of Theoretical Physics, Lund University, Solvegatan 14A, 223 62 Lund, Sweden

§ Institute für Festkörperforschung des Forschungszentrum Jülich, D-52425 Jülich, Germany

Received 23 July 1996

Abstract. A generalization of the local density approximation (LDA) method for systems with strong Coulomb correlations is described which gives a correct description of the Mott insulators. The LDA + U method takes into account orbital dependence of the Coulomb and exchange interactions which is absent in the LDA. The scheme can be regarded as a 'first-principles' method because there are no adjustable parameters. When applied to the transition metal and rare-earth metal compounds, the LDA + U method gives a qualitative improvement compared with the LDA not only for excited-state properties such as energy gaps but also for ground-state properties such as magnetic moments and interatomic exchange parameters. The orbital-dependent rotationally invariant LDA + U potential gives a correct orbital polarization and a corresponding Jahn–Teller distortion as well as polaron formation.

1. Introduction

There are two ways to study the ground-state properties and excitation spectrum of a many-electron system. The first one is to choose some model with one or more adjustable parameters, to calculate with this model some measurable property, for example the spectrum, and to fit the result to the experimental data to determine the parameters of the model. The second one is to find eigenfunctions and eigenvalues of the Hamiltonian in a parameter-free approximation (the first-principles approach). Naturally, the first-principles approach is more appealing, since it has no adjustable parameters. Unfortunately, except for for small molecules, it is impossible to solve the many-electron problem without severe approximations. The most successful first-principles method is the density functional theory (DFT) within the local (spin-) density approximation (L(S)DA) [1], where the many-body problem is mapped into a non-interacting system with a one-electron exchange–correlation potential which is approximated by that of the homogeneous electron gas. LDA has proved to be very efficient for extended systems, such as large molecules and solids.

But, as an approximation, the LDA cannot be successful for all systems although the exact DFT should be capable of obtaining ground-state properties. Strongly correlated materials are examples where deficiency of the LDA is seen most clearly. Such systems usually contain transition metal or rare-earth metal ions with partially filled d (or f) shells. When applying a one-electron method with an orbital-independent potential, like in the LDA, to transition metal compounds, one has as a result a partially filled d band with metallic-type electronic structure and itinerant d electrons. This is definitely a wrong answer for the

0953-8984/97/040767+42$19.50

late-transition-metal oxides and rare-earth metal compounds where d (f) electrons are well localized and there is a sizable energy separation between occupied and unoccupied subbands (the lower Hubbard band and upper Hubbard band in a model Hamiltonian approach).

There were several attempts to improve on the LDA in order to take into account strong electron–electron correlations. One of the most popular approaches is the self-interaction correction (SIC) method [2]. It reproduces quite well the localized nature of the d (or f) electrons in transition metal (rare-earth metal) compounds, but SIC one-electron energies are usually in strong disagreement with spectroscopy data (for example for transition metal oxides occupied d bands are $\approx$1 Ryd below the oxygen valence band).

The Hartree–Fock (HF) method [3] is appropriate for describing Mott insulators because it explicitly contains a term which cancels the self-interaction. The fact that the problem of self-interaction is treated in an averaged way in the LDA is the main reason for which the LDA spectra are in such strong qualitative disagreement with experimental data. However, a serious problem of the Hartree–Fock approximation is the unscreened nature of the Coulomb interaction used in this method. The 'bare' value of Coulomb interaction parameter U is rather large (15–20 eV) while screening in a solid leads to much smaller values: 8 eV or less [4, 5]. Due to the neglect of screening, the HF energy gap values are a factor of 2–3 larger than the experimental values [3].

The problem of screening is addressed in a rigorous way in the GW approximation (GWA) [6, 7] which may be regarded as a Hartree–Fock theory with a frequency- and orbital-dependent screened Coulomb interaction. The GWA has been applied with success to real systems ranging from simple metals to transition metals but applications to more complex systems have not been feasible up to now due to the large computational task. Another problem in using the GW approximation is that in its practical realization [8] a response function, needed to calculate the screened interaction, is computed with the help of the energy bands and wave functions obtained in the LDA calculation. While such a procedure is justified for the systems where correlation effects are small (such as semiconductors [9]), for strongly correlated systems one may need a better starting Hamiltonian than the LDA. This, for example, can be achieved by improving the LDA Hamiltonian using the calculated self-energy in a self-consistent procedure [10].

In the present review, the so-called LDA+U method [11–13] is described where the non-local and energy-dependent self-energy is approximated by a frequency-independent but non-local screened Coulomb potential. A similar approximation is used in a model Hamiltonian approach, which has proved to be successful in applications to strongly correlated systems [14, 15].

2. The LDA + U method

As in the Anderson model [16] we separate electrons into two subsystems: localized d or f electrons for which Coulomb d–d interaction should be taken into account by a term $\frac{1}{2}U\sum_{i\neq j} n_i n_j$ (n_i are d-orbital occupancies) as in a mean-field (Hartree–Fock) approximation, and delocalized s, p electrons which could be described by using an orbital-independent one-electron potential (LDA). Let us consider a d ion as an open system with a fluctuating number of d electrons. If we assume that the Coulomb energy of d–d interactions as a function of total number of d electrons $N = \sum n_i$ given by the LDA is a good approximation (but not the orbital energies (eigenvalues)!), then the correct formula for this energy is $E = UN(N-1)/2$. Let us subtract this expression from the LDA total-energy functional and add a Hubbard-like term (neglecting for a while exchange and non-sphericity).

As a result we have the following functional:

$$E = E_{LDA} - UN(N-1)/2 + \frac{1}{2}U\sum_{i\neq j} n_i n_j \ . \tag{1}$$

The orbital energies ϵ_i are derivatives of (1) with respect to orbital occupations n_i:

$$\epsilon_i = \partial E/\partial n_i = \epsilon_{LDA} + U\left(\frac{1}{2} - n_i\right). \tag{2}$$

This simple formula shifts the LDA orbital energy by $-U/2$ for occupied orbitals ($n_i = 1$) and by $+U/2$ for unoccupied orbitals ($n_i = 0$). A similar formula is found for the orbital-dependent potential ($V_i(\boldsymbol{r}) = \delta E/\delta n_i(\boldsymbol{r})$ where a variation is taken not on the total charge density $n(\boldsymbol{r})$ but on the charge density of a particular ith orbital $n_i(\boldsymbol{r})$):

$$V_i(\boldsymbol{r}) = V_{LDA}(\boldsymbol{r}) + U\left(\frac{1}{2} - n_i\right). \tag{3}$$

The LDA$+U$ orbital-dependent potential (3) gives upper and lower Hubbard bands with the energy separation between them equal to the Coulomb parameter U, thus reproducing qualitatively the correct physics for Mott–Hubbard insulators. To construct a quantitatively sound calculational scheme, one needs to define in a more general way an orbital basis set and to take into account properly the direct and exchange Coulomb interactions inside a partially filled d (or f) atomic shell.

All one needs physically is the identification of regions in space where the atomic characteristics of the electronic states have largely survived ('atomic spheres'), which is not a problem for at least d or f electrons. Within these atomic spheres one can expand in a localized orthonormal basis $|inlm\sigma\rangle$ (i denotes the site, n the main quantum number, l the orbital quantum number, m the magnetic quantum number and σ the spin index). Although not strictly necessary, let us specialize to the usual situation where only a particular nl-shell is partly filled. The density matrix is defined by

$$n^{\sigma}_{mm'} = -\frac{1}{\pi}\int^{E_F} \mathrm{Im}\, G^{\sigma}_{inlm,inlm'}(E)\ \mathrm{d}E \tag{4}$$

where $G^{\sigma}_{inlm,inlm'}(E) = \langle inlm\sigma|(E - \widehat{H})^{-1}|inlm'\sigma\rangle$ are the elements of the Green function matrix in this localized representation, while $\widehat{H}$ will be defined later on. In terms of the elements of this density matrix $\{n^{\sigma}\}$, the generalized LDA + U functional [13] is defined as follows:

$$E^{LDA+U}[\rho^{\sigma}(\boldsymbol{r}), \{n^{\sigma}\}] = E^{LSDA}[\rho^{\sigma}(\boldsymbol{r})] + E^{U}[\{n^{\sigma}\}] - E_{dc}[\{n^{\sigma}\}] \tag{5}$$

where $\rho^{\sigma}(\boldsymbol{r})$ is the charge density for spin-σ electrons and $E^{LSDA}[\rho^{\sigma}(\boldsymbol{r})]$ is the standard LSDA (local spin-density approximation) functional. Equation (5) asserts that the LSDA suffices in the absence of orbital polarizations, while the latter are driven by

$$\begin{aligned} E^{U}[\{n\}] = \frac{1}{2}\sum_{\{m\},\sigma}\{&\langle m, m''|V_{ee}|m', m'''\rangle n^{\sigma}_{mm'} n^{-\sigma}_{m''m'''} \\ &- (\langle m, m''|V_{ee}|m', m'''\rangle - \langle m, m''|V_{ee}|m''', m'\rangle) n^{\sigma}_{mm'} n^{\sigma}_{m''m'''}\} \end{aligned} \tag{6}$$

where V_{ee} are the screened Coulomb interactions among the nl-electrons. Finally, the last term in equation (5) corrects for double counting (in the absence of orbital polarizations, equation (5) should reduce to E^{LSDA}) and is given by

$$E_{dc}[\{n^{\sigma}\}] = \frac{1}{2}UN(N-1) - \frac{1}{2}J[N^{\uparrow}(N^{\uparrow}-1) + N^{\downarrow}(N^{\downarrow}-1)] \tag{7}$$

were $N^\sigma = \mathrm{Tr}(n^\sigma_{mm'})$ and $N = N^\uparrow + N^\downarrow$. U and J are screened Coulomb and exchange parameters [4, 5].

In addition to the usual LDA potential, we find an effective single-particle potential to be used in the effective single-particle Hamiltonian:

$$\widehat{H} = \widehat{H}_{LSDA} + \sum_{mm'} |inlm\sigma\rangle V^\sigma_{mm'} \langle inlm'\sigma| \tag{8}$$

$$V^\sigma_{mm'} = \sum_{\{m\}} \{\langle m, m''|V_{ee}|m', m'''\rangle n^{-\sigma}_{m''m'''} - (\langle m, m''|V_{ee}|m', m'''\rangle - \langle m, m''|V_{ee}|m''', m'\rangle) n^\sigma_{m''m'''}\} - U\left(N - \frac{1}{2}\right) + J\left(N^\sigma - \frac{1}{2}\right). \tag{9}$$

The V_{ee}s remain to be determined. We again follow the spirit of the LDA+U method by assuming that within the atomic spheres these interactions retain largely their atomic nature. Moreover, it is asserted that the LSDA itself suffices to determine their values, following the well-tested procedure of the so-called supercell LSDA approach [4]: the elements of the density matrix $n^\sigma_{mm'}$ have to be constrained locally and the second derivative of the LSDA energy with respect to the variation of the density matrix yields the wanted interactions. In more detail, the matrix elements can be expressed in terms of complex spherical harmonics and effective Slater integrals F^k [17] as

$$\langle m, m''|V_{ee}|m', m'''\rangle = \sum_k a_k(m, m', m'', m''') F^k \tag{10}$$

where $0 \leqslant k \leqslant 2l$ and

$$a_k(m, m', m'', m''') = \frac{4\pi}{2k+1} \sum_{q=-k}^{k} \langle lm|Y_{kq}|lm'\rangle \langle lm''|Y^*_{kq}|lm'''\rangle.$$

For d electrons one needs F^0, F^2 and F^4 and these can be linked to the Coulomb and Stoner parameters U and J obtained from the LSDA supercell procedures via $U = F^0$ and $J = (F^2 + F^4)/14$, while the ratio F^2/F^4 is to a good accuracy a constant $\sim$0.625 for the 3d elements [18, 12]. (For f electrons the corresponding expression is $J = (286F^2 + 195F^4 + 250F^6)/6435$.)

The new Hamiltonian in equation (8) contains an orbital-dependent potential in equation (9) in the form of a projection operator. This means that the LDA + U method is essentially dependent on the choice of the set of the localized orbitals in this operator. That is a consequence of the basic Anderson-model-like ideology of the LDA + U approach: the separation of the total variational space into a localized d- (f-) orbital subspace, with Coulomb interaction between them treated with a Hubbard-type term in the Hamiltonian, and the subspace of all other states for which the local density approximation for Coulomb interaction is regarded as sufficient. The arbitrariness of the choice of the localized orbitals is not as crucial as might be expected. The d (f) orbitals for which Coulomb correlation effects are important are indeed well localized in space and retain their atomic character in a solid. The experience of using the LDA+U approximation in various electronic structure calculational schemes shows that the results are not sensitive to the particular form of the localized orbitals.

Due to the presence of the projection operator in the LDA + U Hamiltonian in equation (8), the most straightforward calculational scheme would be to use atomic-orbital-type basis sets, such as the LMTOs (linear muffin-tin orbitals) [19]. However, as soon as localized d orbitals (f orbitals) are defined, the Hamiltonian in equation (8) can be realized even in schemes using plane waves as a basis set, such as pseudopotential methods.

3. The relationship between the LDA + U and GW methods

Although there is no theoretical justification, it is customary to interpret the Kohn–Sham (KS) eigenvalues in the DFT as quasiparticle energies measured in photoemission experiments. A proper way of calculating quasiparticle energies is provided by the Green function theory. In this approach, the many-body effects are contained in the self-energy operator Σ which is non-local and energy dependent:

$$H_0(\boldsymbol{r})\Psi(\boldsymbol{r}) + \int \mathrm{d}\boldsymbol{r}_1 \; \Sigma(\boldsymbol{r}, \boldsymbol{r}_1, E)\Psi(\boldsymbol{r}_1) = E\Psi(\boldsymbol{r}) \tag{11}$$

where H_0 contains the kinetic energy, the Hartree potential and a possible one-particle external potential. We can think of the DFT exchange–correlation potential V_{xc} as a a local and energy-independent approximation to the self-energy which gives the correct ground-state density. However, in some cases, the non-locality (orbital dependence) and energy dependence are crucial for obtaining excitation spectra.

Unfortunately, the self-energy is very hard to calculate and we have to resort to approximations. The simplest approximation to the self-energy, derived from the many-body perturbation theory, is the GW approximation [6, 7]. But even in this simplest approximation, the computational effort required is already quite large.

It can be shown that the GWA and LDA+U theories are both Hartree–Fock-like theories and, at least for localized states, such as d or f orbitals of transition metal or rare-earth metal ions, the LDA + U theory may be regarded as an approximation to the GWA.

The GWA is given by

$$\Sigma(\boldsymbol{r}, \boldsymbol{r}'; \omega) = \frac{\mathrm{i}}{2\pi} \int_{-\infty}^{\infty} \mathrm{d}\omega' \; G(\boldsymbol{r}, \boldsymbol{r}'; \omega + \omega')W(\boldsymbol{r}, \boldsymbol{r}'; \omega')\mathrm{e}^{\mathrm{i}\delta\omega'}. \tag{12}$$

W is a screened Coulomb potential obtained from the inverse dielectric function:

$$\epsilon^{-1}(\boldsymbol{r}, \boldsymbol{r}'; \omega) = \delta(\boldsymbol{r} - \boldsymbol{r}') + \int \mathrm{d}^3\boldsymbol{r}'' \; v(\boldsymbol{r}' - \boldsymbol{r}'')P(\boldsymbol{r}'', \boldsymbol{r}'; \omega) \tag{13}$$

where P is the full response function. We then have

$$W(\boldsymbol{r}, \boldsymbol{r}'; \omega) = \int \mathrm{d}^3\boldsymbol{r}'' \; \epsilon^{-1}(\boldsymbol{r}, \boldsymbol{r}''; \omega)v(\boldsymbol{r}'' - \boldsymbol{r}') = v(\boldsymbol{r} - \boldsymbol{r}') + W_c(\boldsymbol{r}, \boldsymbol{r}'; \omega) \tag{14}$$

where

$$W_c(\boldsymbol{r}, \boldsymbol{r}'; \omega) = \int \mathrm{d}^3\boldsymbol{r}_1 \; \mathrm{d}^3\boldsymbol{r}_2 \; v(\boldsymbol{r}' - \boldsymbol{r}_1)P(\boldsymbol{r}_1, \boldsymbol{r}_2; \omega)v(\boldsymbol{r}_2 - \boldsymbol{r}'). \tag{15}$$

The time-ordered Green function may be written in the spectral representation:

$$G(\boldsymbol{r}, \boldsymbol{r}'; \omega) = \int_{-\infty}^{\mu} \mathrm{d}\omega' \; \frac{A(\boldsymbol{r}, \boldsymbol{r}'; \omega')}{\omega - \omega' - \mathrm{i}\delta} + \int_{\mu}^{\infty} \mathrm{d}\omega' \; \frac{A(\boldsymbol{r}, \boldsymbol{r}'; \omega')}{\omega - \omega' + \mathrm{i}\delta} \tag{16}$$

where

$$A(\boldsymbol{r}, \boldsymbol{r}'; \omega) = -\frac{1}{\pi}\mathrm{Im}\; G(\boldsymbol{r}, \boldsymbol{r}'; \omega)\; \mathrm{sgn}(\omega - \mu). \tag{17}$$

In practice we use a zeroth-order Green function, so

$$A(\boldsymbol{r}, \boldsymbol{r}'; \omega) = \sum_{kn} \psi_{kn}(\boldsymbol{r})\psi^*_{kn}(\boldsymbol{r}')\delta(\omega - \epsilon_{kn}). \tag{18}$$

The self-energy can now be evaluated and we obtain

$$\Sigma(\boldsymbol{r}, \boldsymbol{r}'; \omega) = \Sigma_x(\boldsymbol{r}, \boldsymbol{r}') + \Sigma_c(\boldsymbol{r}, \boldsymbol{r}'; \omega) \tag{19}$$

where Σ_x is the bare exchange potential

$$\Sigma_x(\boldsymbol{r}, \boldsymbol{r}') = -\sum_{\boldsymbol{k}n}^{occ} \psi_{\boldsymbol{k}n}(\boldsymbol{r})\psi^*_{\boldsymbol{k}n}(\boldsymbol{r}')v(\boldsymbol{r} - \boldsymbol{r}') \tag{20}$$

and Σ_c is the correlated part of the self-energy given by

$$\Sigma_c(\boldsymbol{r}, \boldsymbol{r}'; \omega) = \sum_{\boldsymbol{k}n}^{occ} \psi_{\boldsymbol{k}n}(\boldsymbol{r})\psi^*_{\boldsymbol{k}n}(\boldsymbol{r}')W_c^-(\boldsymbol{r}, \boldsymbol{r}'; \omega - \epsilon_{\boldsymbol{k}n}) + \sum_{\boldsymbol{k}n}^{unocc} \psi_{\boldsymbol{k}n}(\boldsymbol{r})\psi^*_{\boldsymbol{k}n}(\boldsymbol{r}')W_c^+(\boldsymbol{r}, \boldsymbol{r}'; \omega - \epsilon_{\boldsymbol{k}n}) \tag{21}$$

where

$$W_c^{\pm}(\boldsymbol{r}, \boldsymbol{r}'; \omega) = \frac{\mathrm{i}}{2\pi}\int_{-\infty}^{\infty} \mathrm{d}\omega' \, \frac{W_c(\boldsymbol{r}, \boldsymbol{r}'; \omega')}{\omega + \omega' \pm \mathrm{i}\delta}. \tag{22}$$

In short we can write

$$\Sigma(\boldsymbol{r}, \boldsymbol{r}'; \omega) = -\sum_{\boldsymbol{k}n} \psi_{\boldsymbol{k}n}(\boldsymbol{r})\psi^*_{\boldsymbol{k}n}(\boldsymbol{r}')W_0(\boldsymbol{r}, \boldsymbol{r}'; \omega - \epsilon_{\boldsymbol{k}n}) \tag{23}$$

where

$$W_0(\boldsymbol{r}, \boldsymbol{r}'; \omega - \epsilon_{\boldsymbol{k}n}) \equiv [v(\boldsymbol{r} - \boldsymbol{r}') - W_c^-(\boldsymbol{r}, \boldsymbol{r}'; \omega - \epsilon_{\boldsymbol{k}n})]\theta(\mu - \epsilon_{\boldsymbol{k}n}) - W_c^+(\boldsymbol{r}, \boldsymbol{r}'; \omega - \epsilon_{\boldsymbol{k}n})\theta(\epsilon_{\boldsymbol{k}n} - \mu). \tag{24}$$

The self-energy in the GWA has the same form as that in the HFA except that it depends on the energy and contains a term which depends on unoccupied states as a consequence of correlation effects. Thus the GWA can be interpreted as a generalization of the Hartree–Fock approximation (HFA) with a potential W_0 which contains dynamical screening of the Coulomb potential. Note, however, that W_0 is not the same as the dynamically screened potential W.

The LDA + U theory is designed to give the self-energy correction to localized states embedded in delocalized states. The localized states have a large Coulomb correlation which is accounted for by the U-term whereas the delocalized states are well described by the LDA. To make a connection between the GWA and the LDA + U theory we consider the correlated part of the self-energy in the GWA for an occupied core-like state ψ_d:

$$\langle\psi_d|\Sigma_c(\epsilon_d)|\psi_d\rangle = \langle\psi_d\psi_d|W_c^-(0)|\psi_d\psi_d\rangle + \sum_{\boldsymbol{k}n\neq d}^{occ}\langle\psi_d\psi_{\boldsymbol{k}n}|W_c^-(\epsilon_d - \epsilon_{\boldsymbol{k}n})|\psi_{\boldsymbol{k}n}\psi_d\rangle + \sum_{\boldsymbol{k}n}^{unocc}\langle\psi_d\psi_{\boldsymbol{k}n}|W_c^+(\epsilon_d - \epsilon_{\boldsymbol{k}n})|\psi_{\boldsymbol{k}n}\psi_d\rangle. \tag{25}$$

Strictly speaking, the self-energy should be evaluated at the new energy $E_d = \epsilon_d +$ self-energy correction and this is understood to be the case here. If ψ_d is localized and well separated in energy from other states, then the first term is evidently much larger than the rest. The last term contains unoccupied Ψ_d states but they are orthogonal to the occupied ones so this term is much smaller than the first. Thus we may make the following approximation:

$$\langle\psi_d|\Sigma_c(\epsilon_d)|\psi_d\rangle \approx \langle\psi_d\psi_d|W_c^-(0)|\psi_d\psi_d\rangle = -\frac{1}{2}\langle\psi_d\psi_d|W_c(0)|\psi_d\psi_d\rangle. \tag{26}$$

The last step can be shown as follows. The correlated part of the screened potential can be written in terms of its spectral representation:

$$W_c(\omega) = \int_{-\infty}^{0} \mathrm{d}\omega' \; \frac{B(\omega')}{\omega - \omega' - \mathrm{i}\delta} + \int_{0}^{\infty} \mathrm{d}\omega' \; \frac{B(\omega')}{\omega - \omega' + \mathrm{i}\delta} \tag{27}$$

where

$$B(\omega) = -\frac{1}{\pi} \mathrm{Im}\; W_c(\omega)\; \mathrm{sgn}(\omega). \tag{28}$$

W_c is an even function of ω so $B(\omega)$ is odd. We can now calculate

$$W_c(0) = \int_{-\infty}^{0} \mathrm{d}\omega' \; \frac{B(\omega')}{-\omega' - \mathrm{i}\delta} + \int_{0}^{\infty} \mathrm{d}\omega' \; \frac{B(\omega')}{-\omega' + \mathrm{i}\delta} = -2\int_{0}^{\infty} \mathrm{d}\omega' \; \frac{B(\omega')}{\omega' - \mathrm{i}\delta} \tag{29}$$

using the fact that $B(\omega)$ is odd, and

$$\begin{aligned} W_c^-(0) &= \frac{\mathrm{i}}{2\pi} \int_{-\infty}^{\infty} \mathrm{d}\omega' \; \frac{W_c(\omega')}{\omega' - \mathrm{i}\delta} \\ &= \frac{\mathrm{i}}{2\pi} \int_{-\infty}^{\infty} \mathrm{d}\omega' \; \frac{1}{\omega' - \mathrm{i}\delta} \left\{ \int_{-\infty}^{0} \mathrm{d}\omega'' \; \frac{B(\omega'')}{\omega' - \omega'' - \mathrm{i}\delta} + \int_{0}^{\infty} \mathrm{d}\omega'' \; \frac{B(\omega'')}{\omega' - \omega'' + \mathrm{i}\delta} \right\} \\ &= \int_{0}^{\infty} \mathrm{d}\omega'' \; \frac{B(\omega'')}{\omega'' - \mathrm{i}\delta} = -\frac{1}{2} W_c(0). \end{aligned} \tag{30}$$

This is a correction due to the work done on the electron by the polarization field from zero to $W_c(0)$ [6]. A similar result

$$+\frac{1}{2}\langle \psi_d \psi_d | W_c(0) | \psi_d \psi_d \rangle$$

is obtained for an unoccupied core-like state of the same character, so the energy separation of the states is

$$\begin{aligned} \Delta = \epsilon_2^{HF} - \epsilon_1^{HF} + \langle \psi_d \psi_d | W_c(0) | \psi_d \psi_d \rangle &= \langle \psi_d \psi_d | v | \psi_d \psi_d \rangle + \langle \psi_d \psi_d | W_c(0) | \psi_d \psi_d \rangle \\ &= \langle \psi_d \psi_d | W(0) | \psi_d \psi_d \rangle \end{aligned} \tag{31}$$

which agrees with the intuitive result that the 'gap' is given by the screened Coulomb interaction: $\Delta = U \approx W(0)$.

Within the above approximation, the GW self-energy for a localized state is given by

$$\Sigma(\boldsymbol{r}, \boldsymbol{r}'; \epsilon_d) = \Sigma_x(\boldsymbol{r}, \boldsymbol{r}') + \sum_{\boldsymbol{k}n=d} \psi_{\boldsymbol{k}n}(\boldsymbol{r}) \psi^*_{\boldsymbol{k}n}(\boldsymbol{r}') W_c^0(\boldsymbol{r}, \boldsymbol{r}'; \epsilon_d) \tag{32}$$

with

$$W_c^0(\boldsymbol{r}, \boldsymbol{r}'; \epsilon_d) = -\frac{1}{2} W_c(\boldsymbol{r}, \boldsymbol{r}'; 0)[\theta(\mu - \epsilon_d) - \theta(\epsilon_d - \mu)]. \tag{33}$$

It is clear that the self-energy correction to the LDA

$$\Delta\Sigma(\boldsymbol{r}, \boldsymbol{r}'; \epsilon_d) = \Sigma(\boldsymbol{r}, \boldsymbol{r}'; \epsilon_d) - V_{xc}^{LDA}(\boldsymbol{r}) \delta(\boldsymbol{r} - \boldsymbol{r}') \tag{34}$$

should be equated to the U-term in the LDA + U scheme. In the spirit of the LDA + U scheme and the Anderson impurity model, let us divide the space into localized states $\{\phi_m\}$, such as d or f states, and delocalized states $\{\psi_{\boldsymbol{k}n}\}$:

$$\delta(\boldsymbol{r} - \boldsymbol{r}') = \sum_m \phi_m(\boldsymbol{r}) \phi^*_m(\boldsymbol{r}') + \sum_{\boldsymbol{k}n} \psi_{\boldsymbol{k}n}(\boldsymbol{r}) \psi^*_{\boldsymbol{k}n}(\boldsymbol{r}'). \tag{35}$$

The self-energy correction can be written as follows:

$$\Delta\Sigma(\boldsymbol{r},\boldsymbol{r}';\epsilon_d) = \sum_{mm'}\phi_m(\boldsymbol{r})\,\Delta\Sigma_{mm'}(\epsilon_d)\,\phi^*_{m'}(\boldsymbol{r}') + \sum_{\boldsymbol{k}nn'}\psi_{\boldsymbol{k}n}(\boldsymbol{r})\,\Delta\Sigma_{nn'}(\epsilon_d)\,\psi^*_{\boldsymbol{k}n'}(\boldsymbol{r}') + \sum_{\boldsymbol{k}nm}\psi_{\boldsymbol{k}n}(\boldsymbol{r})\,\Delta\Sigma_{nm}(\boldsymbol{k},\epsilon_d)\,\phi^*_m(\boldsymbol{r}') + \sum_{kmn}\phi_m(\boldsymbol{r})\,\Delta\Sigma_{mn}(\boldsymbol{k},\epsilon_d)\,\psi^*_{\boldsymbol{k}n}(\boldsymbol{r}'). \tag{36}$$

Since we are interested in the localized states $\{\phi_m\}$, the first term will dominate and therefore

$$\Delta\Sigma(\boldsymbol{r},\boldsymbol{r}';\epsilon_d) \approx \sum_{mm'}\phi_m(\boldsymbol{r})\,\Delta\Sigma_{mm'}(\epsilon_d)\,\phi^*_{m'}(\boldsymbol{r}') \tag{37}$$

where

$$\Delta\Sigma_{mm'}(\epsilon_d) = \langle\phi_m|\Sigma_x - V_{xc}|\phi_{m'}\rangle + \sum_{m''m'''}\langle m, m''|W_c^0|m''', m'\rangle n_{m'',m'''} \tag{38}$$

with

$$n_{m'',m'''} = \sum_{\boldsymbol{k}n=d}\langle\phi_{m''}|\psi_{\boldsymbol{k}n}\rangle\langle\psi_{\boldsymbol{k}n}|\phi_{m'''}\rangle. \tag{39}$$

We note that the orbitals $\{\phi_m\}$ can always be chosen to be localized within the atomic spheres. The rest of the self-energy correction is small and if necessary it can be incorporated into the one-particle term.

Let us suppose that we have a d ion with d orbitals $\psi_{m\sigma}$ only. Within the above approximation, the GW self-energy for a localized state is given by

$$\Sigma(\boldsymbol{r},\boldsymbol{r}';\epsilon_{m\sigma}) = \Sigma_x(\boldsymbol{r},\boldsymbol{r}') + \sum_{m'\sigma'}\psi_{m'\sigma'}(\boldsymbol{r})\psi^*_{m'\sigma'}(\boldsymbol{r}')\,W_c^0(\boldsymbol{r},\boldsymbol{r}';\epsilon_{m\sigma}) \tag{40}$$

with

$$W_c^0(\boldsymbol{r},\boldsymbol{r}';\epsilon_{m\sigma}) = -\frac{1}{2}W_c(\boldsymbol{r},\boldsymbol{r}';0)[\theta(\mu-\epsilon_{m\sigma}) - \theta(\epsilon_{m\sigma}-\mu)]. \tag{41}$$

What will be the matrix element of the total potential of the electron–electron interaction in the GWA?

$$\begin{aligned}\langle\psi_{m\sigma}|V_{Hartree} + \Sigma_x + \Sigma_c|\psi_{m\sigma}\rangle &= \sum_{m'\sigma'}^{occup}\int\int \mathrm{d}\boldsymbol{r}\;\mathrm{d}\boldsymbol{r}'\;\psi^*_{m\sigma}(\boldsymbol{r})\psi_{m\sigma}(\boldsymbol{r})v(\boldsymbol{r}-\boldsymbol{r}')\psi^*_{m'\sigma'}(\boldsymbol{r}')\psi_{m'\sigma'}(\boldsymbol{r}') \\ &- \sum_{m'}^{occup}\int\int \mathrm{d}\boldsymbol{r}\;\mathrm{d}\boldsymbol{r}'\;\psi^*_{m\sigma}(\boldsymbol{r})\psi_{m'\sigma'}(\boldsymbol{r})v(\boldsymbol{r}-\boldsymbol{r}')\psi_{m\sigma}(\boldsymbol{r}')\psi^*_{m'\sigma'}(\boldsymbol{r}') \\ &+ \left(\frac{1}{2}-n_{m\sigma}\right)\sum_{m'}\int\int \mathrm{d}\boldsymbol{r}\;\mathrm{d}\boldsymbol{r}'\;\psi^*_{m\sigma}(\boldsymbol{r})\psi_{m'\sigma'}(\boldsymbol{r}) \\ &\times\; W_c(\boldsymbol{r},\boldsymbol{r}',0)\psi_{m\sigma}(\boldsymbol{r}')\psi^*_{m'\sigma'}(\boldsymbol{r}')\end{aligned} \tag{42}$$

where $n_{m\sigma}$ is the occupancy of the $m\sigma$-orbital which is equal to 1 if $\mu-\epsilon_{m\sigma} > 0$ and 0 if $\mu-\epsilon_{m\sigma} < 0$.

The above matrix element can be written in the form

$$V_{m\sigma}^{GWA} = \sum_{m'\sigma'}U^0_{mm'}n_{m'\sigma'} - U^0_{mm}n_{m\sigma} - \sum_{m'\neq m}J_{mm'}n_{m'\sigma} + \left(\frac{1}{2}-n_{m\sigma}\right)\sum_{m'}W_{mm'}$$

where $U^0_{mm'}$ is the *unscreened* Coulomb interaction matrix, $J_{mm'}$ is the exchange matrix and the $W_{mm'}$ are the matrix elements of the correlation potential $W_c(\boldsymbol{r}, \boldsymbol{r}', 0)$. If we define the screening parameter W as

$$W = -\sum_{m'} W_{mm'}$$

then the final formula for the GWA potential matrix element will be

$$V^{GWA}_{m\sigma} = \sum_{m'\sigma'} U^0_{mm'} n_{m'\sigma'} - (U^0_{mm} - W) n_{m\sigma} - \sum_{m' \neq m} J_{mm'} n_{m'\sigma} - \frac{1}{2} W.$$

To write down a GWA-type correction to the LSDA we must express the matrix element of the LSDA potential in the same form as above. As the LSDA is not derived from the orbital–orbital interaction formalism but is given as some effective local orbital-independent potential using the electron density dependence of the Coulomb interaction energy as in the homogeneous electron gas, it is not possible to do it in a rigorous way. Let us look at the energy of the electron–electron interaction in the d ion as a function of the total number of d electrons N, $E_{LSDA}[\rho(\boldsymbol{r})] = E_{LSDA}[N|\psi_{m\sigma}(\boldsymbol{r})|^2]$. It is known that while one-electron eigenvalues are not so good in the LSDA, the total-energy values are in much better agreement with more rigorous calculations. So we can suppose that Hartree–Fock formulae could be a good approximation:

$$\begin{aligned} E_{LSDA}[\rho_\sigma(\boldsymbol{r})] &= E_{LSDA}[N_\sigma|\psi_{m\sigma}(\boldsymbol{r})|^2] \\ &= \frac{1}{2} F^0 N(N-1) - \frac{1}{4} J N(N-2) - \frac{1}{4} J (N_\uparrow - N_\downarrow)^2 \end{aligned} \tag{43}$$

where F^0 is a first Slater integral, J is an exchange parameter and

$$N_\sigma = \sum_m n_{m\sigma} \qquad N = N_\uparrow + N_\downarrow.$$

The LSDA electron interaction potential is a variational derivative of the total energy as a functional of the electron density $\rho(\boldsymbol{r})$:

$$V^\sigma_{LSDA}(\rho(\boldsymbol{r})) = \frac{\delta E_{LSDA}[\rho(\boldsymbol{r})]}{\delta \rho^\sigma(\boldsymbol{r})}.$$

The derivative of the interaction energy as a function of the total number of d electrons N_σ is

$$\begin{aligned} \frac{\partial E_{LSDA}[N_\sigma|\psi_{m\sigma}(\boldsymbol{r})|^2]}{\partial N_\sigma} &= \int \mathrm{d}\boldsymbol{r}\ \frac{\delta E_{LSDA}[\rho(\boldsymbol{r})]}{\delta \rho^\sigma(\boldsymbol{r})} \frac{\partial \rho^\sigma(\boldsymbol{r})}{\partial N_\sigma} = \int \mathrm{d}\boldsymbol{r}\ V^\sigma_{LSDA}(\rho(\boldsymbol{r}))|\psi_{m\sigma}(\boldsymbol{r})|^2 \\ &= F^0 N - \frac{1}{2}(F^0 - J) - J N_\sigma. \end{aligned} \tag{44}$$

That gives us the matrix element of the LSDA potential:

$$V^{LSDA}_{m\sigma} = F^0 N - \frac{1}{2}(F^0 - J) - J N_\sigma$$

The GWA correction to the LSDA potential is:

$$\begin{aligned} \delta V_{m\sigma} &= V^{GWA}_{m\sigma} - V^{LSDA}_{m\sigma} \\ &= \sum_{m'\sigma'} U^0_{mm'} n_{m'\sigma'} - (U^0_{mm} - W) n_{m\sigma} - \sum_{m' \neq m} J_{mm'} n_{m'\sigma} - \frac{1}{2} W \\ &\quad - F^0 \sum_{m'\sigma'} n_{m'\sigma'} + J \sum_m n_{m\sigma} + \frac{1}{2}(F^0 - J) \end{aligned}$$

$$= \sum_{m'\sigma'}(U^0_{mm'} - F^0)n_{m'\sigma'} - (U^0_{mm} - W)n_{m\sigma} - \sum_{m'\neq m} J_{mm'}n_{m'\sigma}$$
$$- \frac{1}{2}W + J\sum_m n_{m\sigma} + \frac{1}{2}(F^0 - J). \tag{45}$$

The difference $U^0_{mm'} - F^0$ does not depend on the Slater integral F^0 (it depends only on the Slater integrals F^k with $k \neq 0$) and is equal to $U_{mm'} - U$ where $U = F^0 - W$ is a screened Coulomb parameter and $U_{mm'}$ is a screened Coulomb matrix.

$$\delta V_{m\sigma} = V^{GWA}_{m\sigma} - V^{LSDA}_{m\sigma}$$
$$= \sum_{m'} U_{mm'}n_{m'-\sigma} + \sum_{m'\neq m}(U_{mm'} - J_{mm'})n_{m'\sigma} - U\left(N - \frac{1}{2}\right) + J\left(N_\sigma - \frac{1}{2}\right). \tag{46}$$

The above formula is equivalent to the LDA + U potential correction equation (9) if the occupation matrix (4) is diagonal:

$$n^\sigma_{mm'} = n_{m\sigma}\delta_{mm'}$$
$$U_{mm'} = \langle m, m'|V_{ee}|m, m'\rangle$$
$$J_{mm'} = \langle m, m'|V_{ee}|m', m\rangle.$$

The only (and the essential) difference is the procedure for calculating the screened Coulomb parameter U. In the LDA + U method it was done by a constrained LSDA supercell calculation and in the GWA it requires the difficult computation of the response function.

We have established a relationship between the GWA and LDA + U theory by recognizing that both are Hartree–Fock-like theories, thus giving a theoretical justification for the latter. At least for localized states, such as d or f states where on-site Coulomb correlation is very important, the LDA + U theory may be regarded as an approximation to the GWA. Whether they give the same results depends on three main things.

(1) How close is the value of U to the static screened potential $W(0)$?

(2) How important is the energy dependence of W which is neglected in the LDA + U theory?

(3) How important is self-consistency which is imposed in the LDA + U calculations but not normally in the GW calculations?

4. Localized states: 3d and 4f orbitals

4.1. Gd

Gd metal is a good test to check how physically sound the approximations are which were used in the derivation of the LDA + U formula presented above. The Gd ion has seven f electrons so the majority-spin subshell is completely filled and the minority-spin subshell is empty. The hybridization of the localized f orbitals with the conduction bands is small and the 4f shell could be regarded with good accuracy as that of the Gd^{3+} ion in the $^8S_{7/2}$ ground state, well separated from all other excited terms. That means that the ground state is well described by a single-Slater-determinant wave function and the LDA + U theory as a one-electron theory is valid here. The final $N - 1$ and $N + 1$ states of the removal (XPS) and addition (BIS) spectra are also well described by a single Slater determinant (^{7}F, neglecting spin–orbit coupling which gives splitting of the order of less than 1 eV). As a

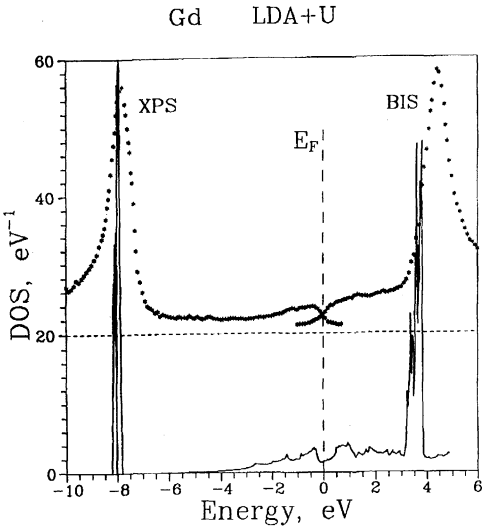

Figure 1. The density of states for ferromagnetic Gd metal from LDA+U calculation and results of BIS (bremsstrahlung isochromat spectroscopy) and XPS (x-ray photoemission spectroscopy) experiments.

result, the theoretical XPS and BIS are (again neglecting spin–orbit coupling) single lines separated by $U + 6J$. The calculation for Gd [20] gives $U = 6.7$ eV and $J = 0.7$ eV thus resulting in a theoretical value of the splitting between occupied and unoccupied 4f bands $\approx$11 eV in good agreement with the experimental value, $\approx$12 eV (figure 1).

The advantage of the LDA + U method is the ability to treat *simultaneously* delocalized conduction band electrons and localized 4f electrons in the same computational scheme. For such a method it is important to be sure that the relative energy positions of these two types of band are reproduced correctly. The example of Gd gives us confidence in this (figure 1): there is a good agreement between calculated and experimental spectra not only for the separation between 4f bands but also for the position of the 4f peaks relative to the Fermi energy. Gd is usually presented as an example where the LSDA gives the correct electronic structure due to the spin-polarization splitting of the occupied and unoccupied 4f bands (in all other rare-earth metals LSDA gives an unphysical 4f peak in the Fermi energy). In the LSDA, the energy separation between 4f bands is not only strongly underestimated (the exchange splitting is only 5 eV instead of the experimental value of 12 eV) but also the unoccupied 4f band is very close to the Fermi energy thus strongly influencing the Fermi surface and magnetic ground-state properties (in the LSDA calculation the antiferromagnetic state is lower in total energy than the ferromagnetic one in contradiction to the experiment). The LDA + U theory solves both of these problems [20].

4.2. Transition metal impurities in alkaline metals

The d orbitals of transition metal ions are much less localized compared with the 4f orbitals of the rare-earth metal ions. The hybridization of the d states between themselves and the s and p states in transition metals results in d-band widths of a few eV. However, there is one case where d shells of transition metal atoms show properties typical for free ions: 3d and 4d impurities introduced into alkali metal hosts by ion implantation [21]. While it is

typical for 3d ions in solids to have local magnetic moments, experimental observation of magnetic moments on 4d impurities in Rb is very unusual. Moreover, there are indications that even the orbital moment is not quenched in these systems.

The reason for this is the large value of the Wigner–Seitz volume of Rb atoms compared with that of transition metal atoms. As a result, the energy of the d states falls to the bottom (or even below the bottom) of the alkali metal conduction band and their hybridization with the hosts states becomes very small, leading to narrow resonant states, similar to the f bands in the rare-earth metals. The calculated impurity density of states [22] has the form of very narrow delta-function-like peaks, thus justifying a discrete-level free-ion description of the electronic structure of these impurities.

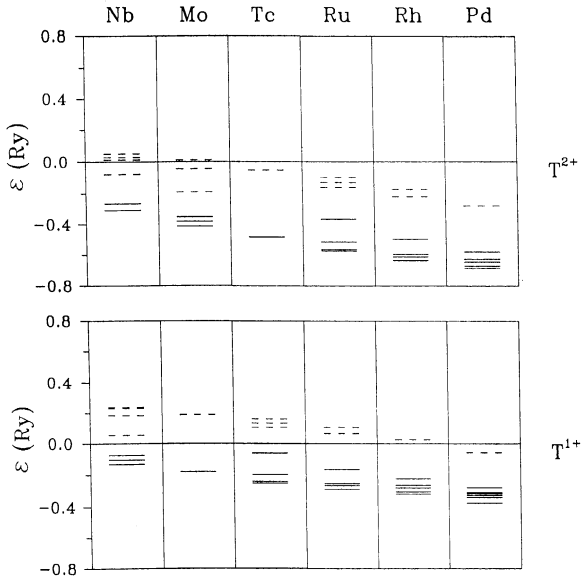

Figure 2. Positions of the one-electron levels with respect to the Fermi energy obtained in the framework of the LDA + U theory for two valence states (T^{2+} and T^{1+}) of 3d impurities in Rb. The solid (dashed) lines were used for the states which were supposed to be occupied (empty) [23].

LDA + U calculations for d impurities in Rb [22, 23] (figure 2) showed that the majority of elements have the T^{1+} valence state (where T is any transition metal), having one d electron more than in a free atom. The Pd impurity has an unusual d^{10} configuration resulting in a non-magnetic state while all other impurities are magnetic, which agrees well with experimental data [21].

4.3. Cerium monopnictides: CeSb

While usually 4f orbitals of rare-earth ions could be regarded as semi-core states, in some rare-earth compounds hybridization of 4f orbitals with other states can be physically important. Examples of such systems are cerium monopnictides with their unusual magnetic properties. Among the pnictides CeSb has a special position. In addition to the anomalies inherent to all monopnictides, CeSb has a large magnetic anisotropy together with a small crystal-field splitting, an extremely complicated magnetic phase diagram, and the largest

known Kerr angle [24].

The standard LSDA approach, where 4f orbitals are treated as band states, fails to predict the ground-state properties: the value of the equilibrium magnetic moment, the additional orbits found in de Haas–van Alphen experiments, and the small density of states at the Fermi level [25]. But exclusion of 4f orbitals from the basis set (treating them as completely localized pseudo-core states) also did not lead to a satisfactory description of electronic and magnetic properties of CeSb. On the other hand, an empirical p–f model with a localized 4f level 2–3 eV below E_F *hybridizing* with the conduction band electrons was able to describe CeSb qualitatively [26].

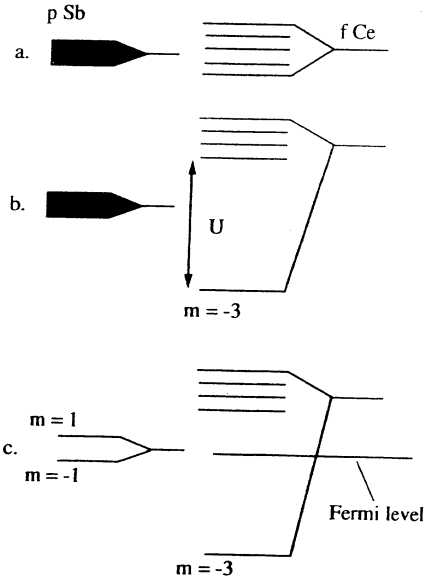

Figure 3. A schematic picture of Hubbard-induced anisotropy formation in the LDA+U scheme for CeSb: (a) normal LDA structure of p and f bands in CeSb; (b) a shift of one f state of Ce (predominantly with $m = -3$ character); (c) the results of strong p–f hybridization and the creation of a highly polarized structure of p states of Sb [20].

The results of the LDA + U calculation for CeSb [27] gave some support to the above-mentioned empirical p–f model. Without spin–orbital coupling, it was found that the Hartree–Fock-like one-electron 4f spin-up states with predominantly $m = 3$ and $m = -3$ character have the lowest total energy. This is in agreement with the first and second of Hund's rules. One should note that the symmetry of such orbitals is not cubic any more and Jahn–Teller tetragonal distortions give a lower energy. The spin–orbital coupling ($\sim$0.5 eV) lifts the degeneracy of the $m = \pm 3$ states according to the third Hund's rule and the lowest energy corresponds to the $|-3\uparrow\rangle$ one-electron state (the spin and orbital moments are equal to $-0.92\mu_B$ and $2.86\mu_B$ yielding a total magnetic moment of $1.94\mu_B$, which is close to the experimental value obtained for the antiferromagnetic ground state, $(2.10 \pm 0.04)\mu_B$ [24] (figure 3).

The band structure of CeSb obtained in the LDA + U calculation (figure 4) has f bands split by approximately 6 eV, and the singly occupied f band is located at 2 eV below the Fermi level. All unoccupied f bands are at approximately 4 eV above E_F and the broad bands which cross the Fermi level are formed by Sb p states. There is a large reduction of

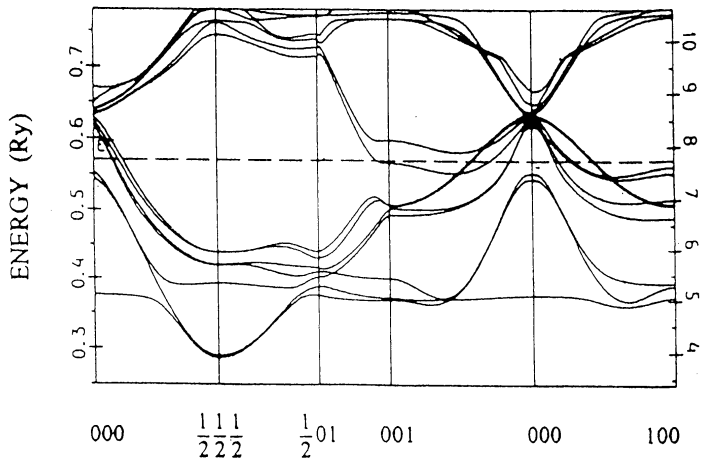

Figure 4. The band structure of ferromagnetically ordered CeSb. Both Rydberg and electron volt scales are shown [27].

Table 1. Experimental (exp) and calculated (LDA + U and LSDA) spin moment (m in μ_B) and energy gap (E in eV) values of the late-3d-transition-metal oxides.

	E_{LSDA}	E_{LDA+U}	E_{exp}	m_{LSDA}	m_{LDA+U}	m_{exp}
$CaCuO_2$	0.0	2.10	1.5	0.0	0.66	0.51
CuO	0.0	1.9	1.4	0.0	0.74	0.65
NiO	0.2	3.1	4.3, 4.0	1.0	1.59	1.77, 1.64, 1.90
CoO	0.0	3.2	2.4	2.3	2.63	3.35, 3.8
FeO	0.0	3.2	2.4	3.4	3.62	3.32
MnO	0.8	3.5	3.6–3.8	4.61	1.67	4.79, 4.58

the density of states at the Fermi level with an LDA + U value of $N(E_F) = 6.5$ states Ryd^{-1} compared to the LSDA value of about 150 states Ryd^{-1}. The occupied f band with mostly $m = -3$ character interacts in a very anisotropic way with Sb p bands and even pushes one of the p states (mostly of $m = 1$ character) above the Fermi level along the Γ–Z direction, but not in the Γ–X direction. This electronic structure leads to an anisotropic Fermi surface (FS) which almost coincides with the FS in the p–f model [26]. The anisotropic p–f interaction helps explain the anomalous magnetic properties of CeSb with strong magnetic anisotropy in the ferromagnetically ordered phase (the calculated value of the magnetic anisotropy as the total-energy difference for the magnetic field along [001] and [110] directions is 2.4 meV (standard LSDA calculations give 0.54 meV)). Such anisotropic p–f mixing for different m-subbands near the Fermi level, together with the large spin–orbital coupling of Sb p states (∼0.6 eV), leads to particularly strong magneto-optical effects.

4.4. $PrBa_2Cu_3O_7$

Another case where the hybridization of the nearly localized f orbitals with the band states near the Fermi level leads to anomalous effects is $PrBa_2Cu_3O_7$. Among all rare earths (RE) that form the $ReBaCu_3O_7$ structure only $PrBa_2Cu_3O_7$ is non-metallic and non-

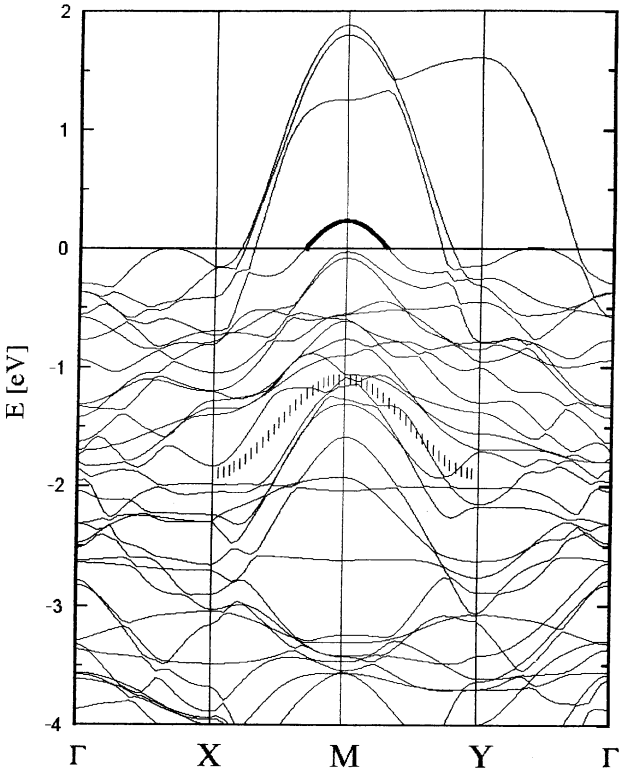

Figure 5. The LDA + U electron band structure of $PrBa_2Cu_3O_7$ for the majority spin. The thick line shows the depleted part of the Fehrenbacher–Rice band. The hatched strip indicates the position of this band in the spin-minority channel (or in $YBa_2Cu_3O_7$) [29].

superconducting. The only satisfactory model which qualitatively explains this puzzle is that of Fehrenbacher and Rice [28] which assumes a hole depletion in the CuO_2 planes due to the transfer of holes from the Cu–O pdσ band into a p–f hybridized state which is a mixture of $4f^1$ and $4f^2L$ configurations (L is a ligand hole in the O 2p orbital with $z(x^2 - y^2)$ symmetry around the Pr site and distributed over the eight nearest oxygen sites).

The results of the LDA + U calculation for $PrBa_2Cu_3O_7$ [29] have fully confirmed the Fehrenbacher and Rice model. In this calculation, the correlation correction (equation (9)) was applied to the Pr 4f orbitals only and not to Cu 3d orbitals. The reason for this is that while LDA + U correction to a potential acting on d orbitals is necessary and sufficient for describing the insulating state of transition metal oxides with partially filled d shells [11], transition from an antiferromagnetic insulator to a paramagnetic metal with doping by holes is beyond the scope of the mean-field approximation. This '$Pr - U$-only' calculation was done to describe transfer of holes from the Cu–O pdσ band into the p–f hybridized state.

For $PrBa_2Cu_3O_7$ the LDA + U calculations yield occupied $\sqrt{1-\alpha_{Pr}^2}f^{\uparrow}_{z(x^2-y^2)} + \alpha_{Pr}L^{\uparrow}$ and $f^{\uparrow}_{z(5z^2-3)}$ bands ($\alpha_{Pr} \sim 0.2$), and a partly occupied antibonding $\alpha_{Pr}f^{\uparrow}_{z(x^2-y^2)} + \sqrt{1-\alpha_{Pr}^2}L^{\uparrow}$ band with a cylindrical hole pocket around the SR line ($\pi/a, \pi/b, k_z$) (figure 5). This partly occupied band grabs holes which normally would be in a Cu–O pdσ band thus reducing its effective doping and making its occupation closer to half-filling where the stable electronic

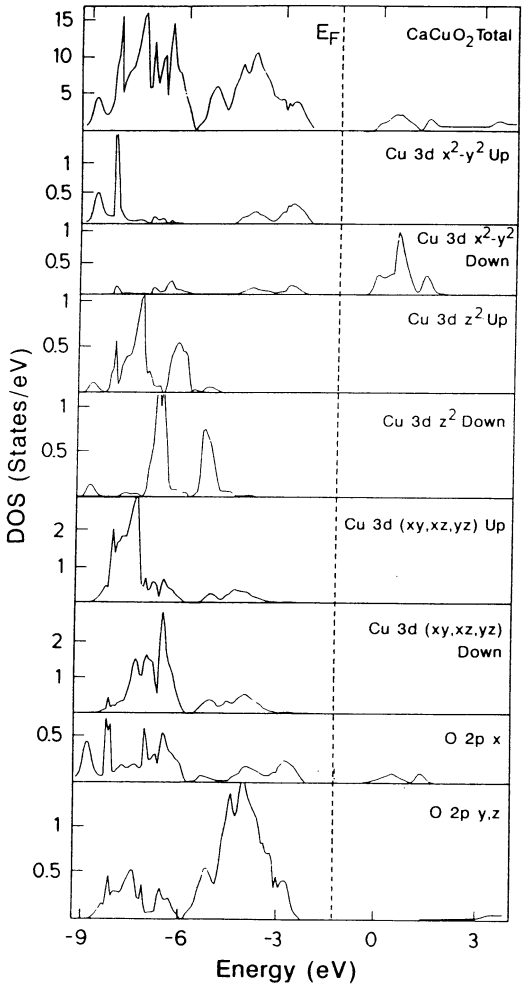

Figure 6. The total and partial densities of states of Cu and O in $CaCuO_2$. O $2p_x$ and O $2p_{y,z}$ refer to the oxygen orbitals pointing towards and perpendicular to the Cu $3d_{x^2-y^2}$ orbitals, respectively [11].

state is known to be an antiferromagnetic insulator. In $NdBaCu_3O_7$, the on-site $f^{\uparrow}_{z(x^2-y^2)}$ electron energy is so low that the top of the antibonding $\alpha_{Nd} f^{\uparrow}_{z(x^2-y^2)} + \sqrt{1-\alpha^2_{Nd}}\, L^{\uparrow}$ band ($\alpha_{Nd} < \alpha_{\mathrm{Pr}}$) has fallen to ~0.3 eV below the Fermi energy E_F. A relatively low degree of doping with Pr could, however, push the top of this band partially above E_F.

5. Mott–Hubbard insulators: transition metal compounds

5.1. 3d-transition-metal oxides

The electronic structure of the rare-earth metal compounds is a relatively simple problem due to the weak hybridization of 4f orbitals with the conduction band states. The advantages of the simultaneous treatment of the localized and delocalized electrons in the LDA + U

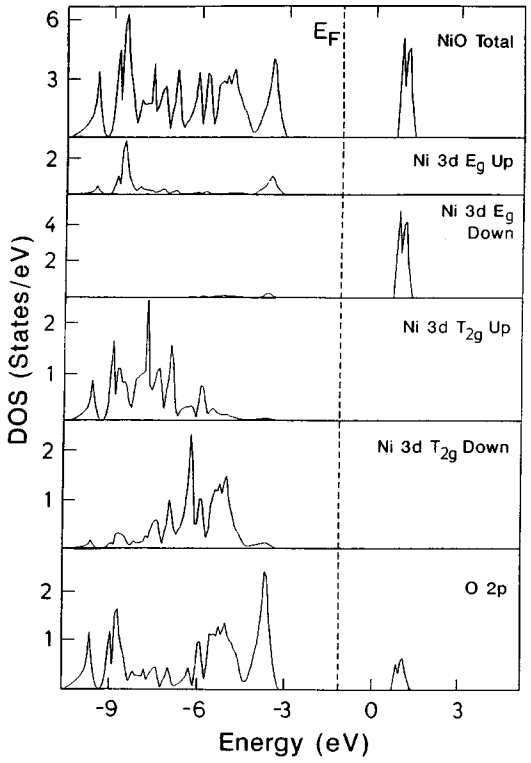

Figure 7. The total and partial densities of states of NiO [11].

method are seen most clearly for the transition metal compounds, where 3d electrons, while remaining localized, hybridize quite strongly with other orbitals. Late-transition-metal oxides, for which LSDA results strongly underestimate the energy gap and magnetic moment values (or even give qualitatively wrong metallic ground states for the insulators CoO and $CaCuO_2$), are well described by the LDA + U method [11] (see table 1).

In figures 6–8 the partial densities of states (DOSs) of $CaCuO_2$, NiO and CoO are shown. The DOSs of FeO and MnO are similar to that of CoO, except for the growing number of unoccupied t_{2g} bands. First, focusing on the unoccupied density of states of NiO (figure 7), one can see that all of the weight is concentrated in the narrow $e_{g\downarrow}$ peak, in agreement with experimentally observed $d^8 \longrightarrow d^9$ peak [30]. In CoO (figure 8) the $3d_{xy\downarrow}$ orbital is emptied too, and this band is located at $\sim$0.5 eV lower energy. This crystal-field splitting of the unoccupied d band is also found experimentally [31]. Comparing now the unoccupied DOS of CoO or NiO with that of $CaCuO_2$, we found that the width of the $3d_{x^2-y^2\downarrow}$ band of the cuprate is larger by a factor of 4–5 compared to that of the rock-salt oxides. As a result, a sharp $d^9 \longrightarrow d^{10}$ peak is missing, which is in striking agreement with experiment [32]. This is obviously related to the formation of a broad Cu $3d_{x^2-y^2}-$O 2p band caused by the relatively small in-plane Cu–O bond length and a Cu–O–Cu bond angle of 180°. In CuO, on the other hand, the bond angles are much smaller (between 96° and 146°) so two neighbouring Cu $3d_{x^2-y^2}$ orbitals hardly couple via the same ($2p_x$ or $2p_y$) O orbital. One expects thus a strong decrease of the band width in going from $CaCuO_2$ to CuO [33], despite the similarity of the two systems on a local level [34]. In figure 9,

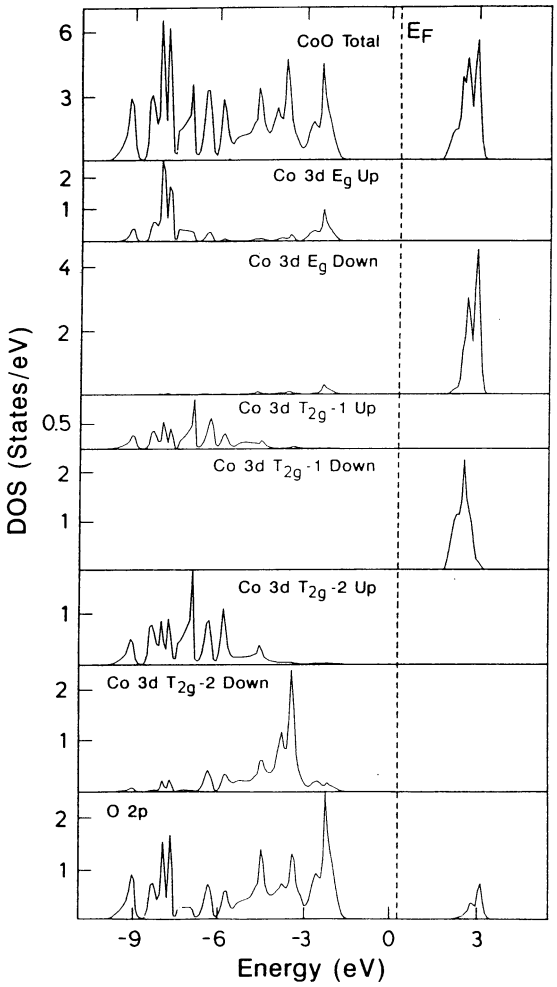

Figure 8. The total and partial densities of states of CoO. Notice the inequivalence of the t_{2g} orbitals, due to the orbital dependence of the LDA + U potentials [11].

the results of the LDA + U calculation for the DOS of CuO are shown. The CuO crystal structure has four equivalent Cu atoms per unit cell. Experimentally, the unoccupied DOS of CuO is characterized by a relatively sharp peak corresponding to the unoccupied d band, which is in strong contrast to the 'blurred' unoccupied DOS of the high-T_c cuprates [35]. The LDA + U results suggest that this difference comes from the smaller band width in the former (figure 9).

In the case of NiO, the LDA + U results are less conventional. In the past the peak at the top of the occupied valence band (corresponding to the lowest-binding-energy (BE) peak in the photoemission spectrum) has been ascribed to the high-spin d^{n-1} state (an additional photoelectron hole in the $t_{2g\downarrow}$ orbital) and the higher-BE shoulder to the low-spin state (a photoelectron hole in the $e_{g\uparrow}$ orbital) [36], and this is also the outcome of several many-body-model calculations [37, 14]. According to our calculations, this high-spin–low-spin identification has to be reversed. The peak at the top of the valence band in NiO is clearly

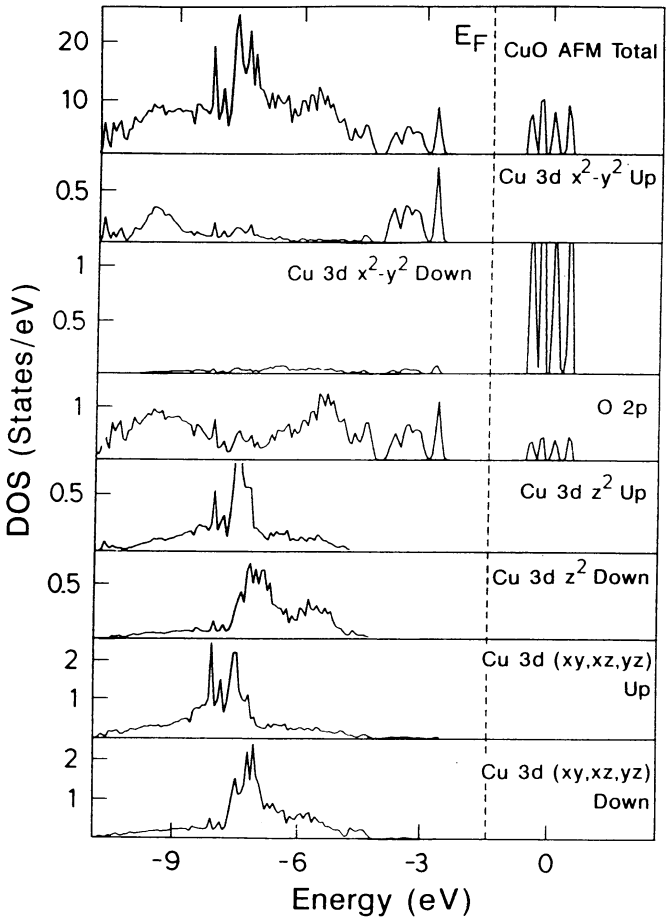

Figure 9. The total and partial densities of states of CuO. Compared to the case for $CaCuO_2$, the unoccupied-, as well as the occupied-local-singlet, band widths are decreased [11].

of $e_{g\uparrow}$ character and of the same sort as for the $3d_{x^2-y^2\uparrow}$ in the cuprates. This low-spin nature of the lowest ionization state of NiO is in agreement with experiment. This follows unambiguously from doping experiments. NiO can be doped with a large concentration of Li, and the Ni(III) compound $LiNiO_2$ is especially well characterized [38]. In this compound, every second (111) plane of Ni is replaced by a plane of Li and the local environment of Ni ions barely changes. $LiNiO_2$ is thus from a local perspective representative for NiO. According to x-ray absorption spectroscopy (XAS) data, the additional holes (introduced by Li doping) have O 2p character [39]. Further, $LiNiO_2$ is a low-spin ($S = \frac{1}{2}$) material [40]. The many-body interpretation is as follows: the added hole goes predominantly in the oxygen band and it gets antiferromagnetically bound to the Ni spin.

The results of LDA + U calculations for $LiNiO_2$ [11] are shown in figure 10 for the most stable (ferromagnetic, ferro-orbital-ordered) ground-state configuration. Compared to NiO, there are some similarities. One still can see a rather narrow $e_{g\downarrow}$ unoccupied 3d band at roughly the same position as in NiO, relative to the first occupied state. The new aspect is that a new unoccupied band of predominantly O 2p character is found inside the 'NiO'

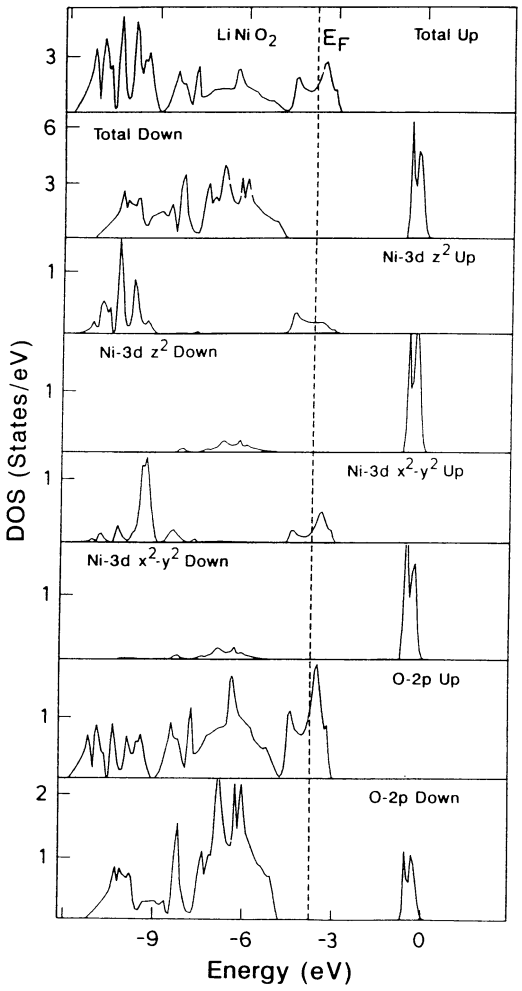

Figure 10. The total and partial densities of states of $LiNiO_2$ [11].

gap, which is centred just above E_F. This is the same pattern as found by Kuiper *et al* [39] in their XAS data. The magnetic moments values are $1.30\mu_B$ and $-0.15\mu_B$ at the Ni and O site, respectively, and the net moment per NiO_2 unit is therefore exactly $1\mu_B$ ($S = \frac{1}{2}$).

5.2. Fe impurity in MgO

The description of the electronic state of 3d impurities in insulators is another example where Coulomb interactions inside the d shell must be properly taken into account in order to cure the deficiency of the LSDA. The ground state of the Fe impurity in MgO [41] is $^5T_2$ (configuration $t_{2g}^4 e_g^2$) thus showing a high-spin magnetic Jahn–Teller ion. However, an LSDA supercell calculation results in a non-magnetic solution with configuration $t_{2g}^6 e_g^0$. The reason for this is that in a magnetic configuration the Fermi level of the LSDA solution crosses two narrow peaks (spin-down t_{2g} and spin-up e_g) and such a solution would be therefore energetically very unfavourable. The orbital-dependent potential of the LDA + U

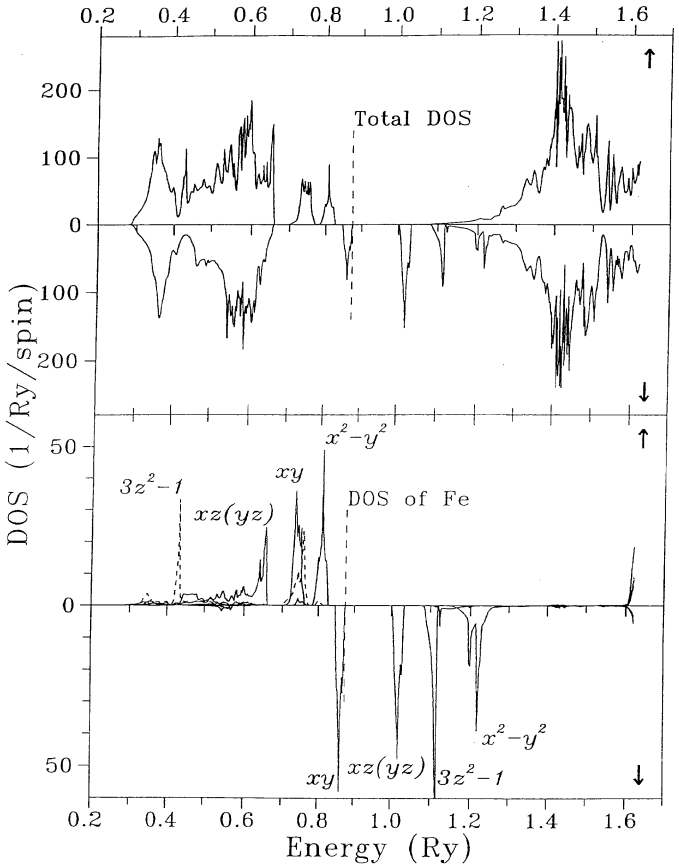

Figure 11. The spin-resolved total density of states (DOS) and local orbital-resolved DOS at the Fe site in $FeMg_7O_8$ for the optimized geometry (LDA + U result) [41].

method splits partially occupied bands and results in a stable insulating magnetic solution with configuration $t_{2g}^4 e_g^2$ (figure 11).

The configuration $t_{2g}^4 e_g^2$ has a partially filled spin-down t_{2g} band and it is known that Fe impurity in MgO exhibits a dynamic Jahn–Teller behaviour. The optimization of the lattice around an impurity atom in the LDA + U calculation agreed quite well with this fact: the total energy has a minimum as a function of tetragonal distortion of the O_6 octahedron for the value of 0.5% of the lattice constant.

Although substitutional Fe in MgO exists mostly as a 2+ ion, the Fe^{3+} configuration is also known to exist. Most probably Fe^{3+} ions are formed due to the trapping of holes at Fe^{2+} sites. A supercell LDA + U calculation with one electron less than the stochiometric value indeed led to the hole being localized on an impurity site with the Fe ion in the Fe^{3+} state (the high-spin $t_{2g}^3 e_g^2$ configuration).

5.3. Linear chain (MX) compounds

The halogen-bridged transition metal linear-chain compounds, referred to as MX compounds because of their alternating transition metal atoms M and halogen atoms X, form weakly

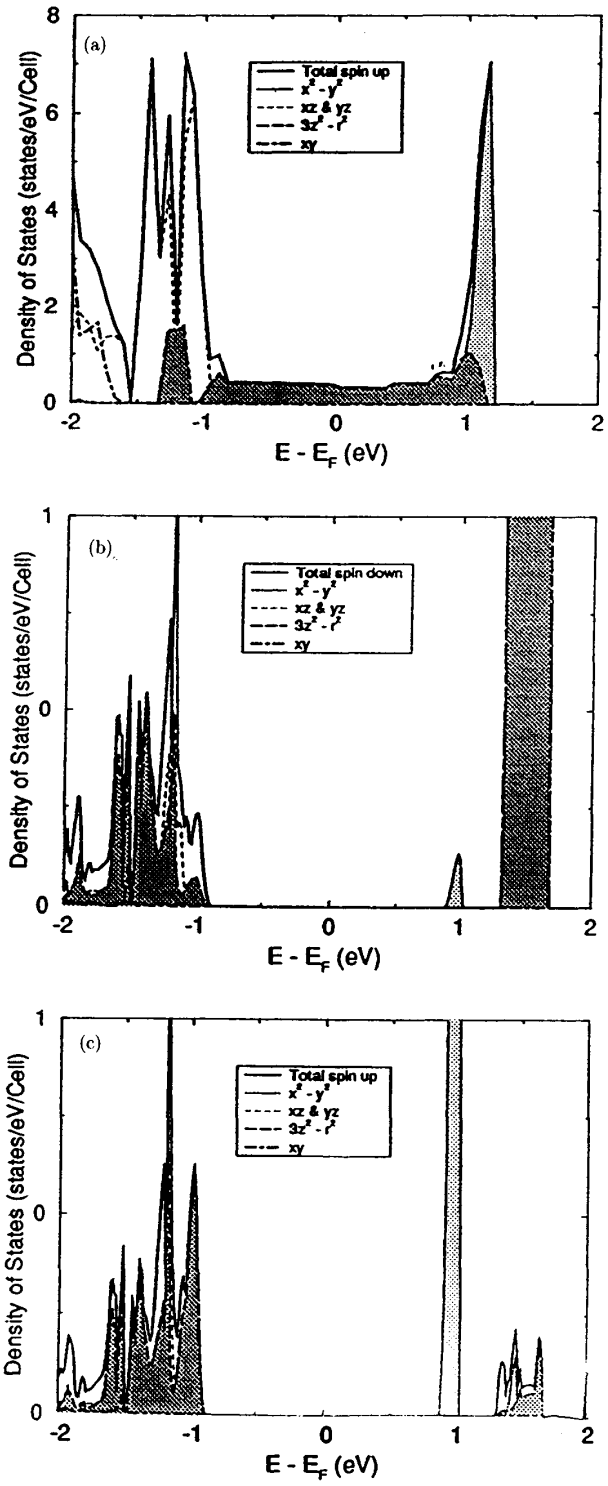

Figure 12. The total and partial densities of states at the Ni site for a Ni-based MX chain compound. (a) The LSDA result; (b), (c) the LDA + U result [43].

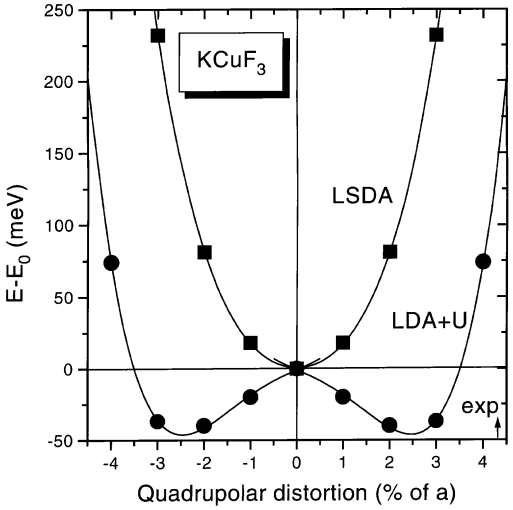

Figure 13. The dependence of the total energy of $KCuF_3$ on the quadrupolar lattice distortion obtained in calculations with LSDA and LDA + U functionals [13].

coupled linear-chain-like structures and are of considerable interest due to a rich phase diagram. They exhibit a charge-density wave (CDW) with dimerization distortion as well as a spin-density wave (SDW) or even a peculiar mixture of them (the spin–Peierls state) [42].

While the LSDA successfully describes CDW systems (for example Pt-based MX compounds) it fails to give the correct antiferromagnetic insulator solution for Ni-based MX predicting instead a non-magnetic metal. This problem has the same origin as for the undoped cuprate superconductor materials: the fact that in the LSDA the magnetic transition is driven by the spin polarization of a Stoner intra-atomic exchange interaction I (about 1 eV), instead of the much stronger Hubbard interaction U (about 8 eV). Again, as was the case with $CaCuO_2$ and La_2CuO_4, using the LDA + U functional gave the correct antiferromagnetic insulating-ground-state Ni-based MX compound [43], while dimerization distortion did not lead to the total energy lowering as it did with the Pt-based systems. It is interesting to note that due to the large ligand-field splitting the Ni^{3+} ion in these compounds has a low-spin ground state (configuration $t_{2g}^6 e_g^1$) (figure 12).

6. Electron–lattice interaction: Jahn–Teller distortions and polarons

We must emphasize here that in spite of the model Hamiltonian spirit in the above derivation of the LDA + U formula, it remains a 'first-principles', '*ab initio*' method preserving its ability to calculate the lattice properties such as the ground-state crystal structure, equilibrium volume and even phonon frequencies. The orbital-dependent potential of the LDA + U method (9) makes it possible to treat properly the orbital polarization and corresponding to it the lattice Jahn–Teller distortions and polarons [13, 44].

6.1. Jahn–Teller distortions: $KCuF_3$

These were demonstrated for the example for the perovskite $KCuF_3$ [13]. This compound is subject to a collective Jahn–Teller-like distortion which is more complicated than the

simple tetragonal distortion of the cuprates, involving a staggering of quadrupolar-distorted CuF_4 units (two short and two long Cu–F bonds) in the a–b planes. In a seminal work, Kugel and Khomskii [45] pointed out that this distortion is in the first instance electronically driven. They showed that the e_g ($x^2 - y^2$, $3z^2 - 1$) orbital degrees of freedom are, like the spins, subject to kinetic exchange interactions, while in addition, the spin and orbital degrees of freedom are mutually coupled as well. Orbital ordering is found from these Hamiltonians involving a staggering of the orbitals in a–b directions ($\sim x^2 - z^2$, $y^2 - z^2$) and a ferromagnetic ordering of the spins. Because of this 'pre-existing', electronically driven orbital polarization, any non-zero electron–phonon interaction then leads automatically to the observed lattice distortion [45].

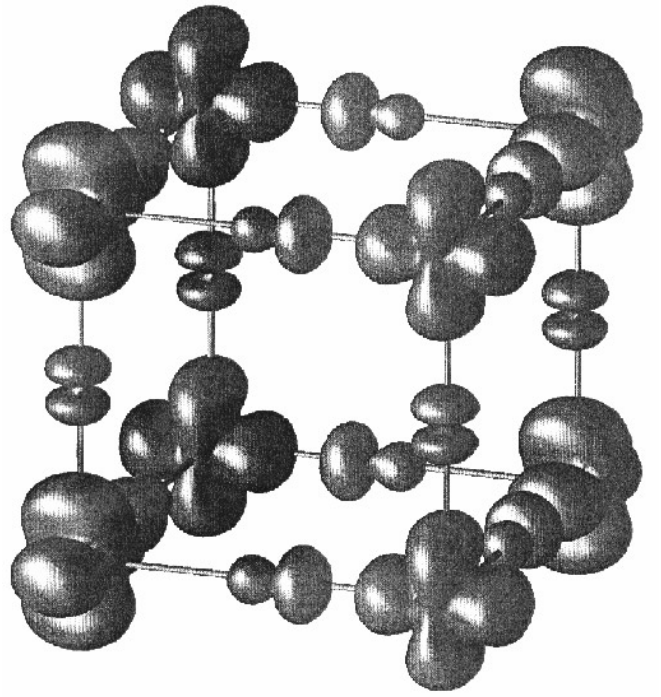

Figure 14. A three-dimensional plot of the electron spin-density distribution in $KCuF_3$ from the results of LDA + U calculations. Note that $x^2 - y^2$- and $y^2 - z^2$-like 'd orbitals' correspond to the spin density located at the copper atoms, while p-like density corresponds to fluorine ions [13].

$KCuF_3$ has the perovskite crystal structure with a slight tetragonal distortion (c/a ratio < 1) while the planes show quadrupolar distortion. The spins are ferromagnetically ordered in the planes while the unit cell is doubled in the c-direction by antiferromagnetic spin ordering, so the resulting unit cell contains four formula units. The primary subject of the investigation [13] was the quadrupolar distortion in planes which is directly connected with the peculiar orbital ordering. The total energy as a function of the shifts of the fluorine ions in the CuF_2 plane was calculated with the standard LSDA and LDA + U functionals (figure 13). The striking difference between the two calculations is that the LSDA solution has no instability against quadrupolar distortion while the LDA+U curve has a minimum at $Q = 2.5\%$ of a compared with the experimental value of 4.4%. This means that exchange-only and lattice–electron ('electron–phonon') interactions in the LSDA are not enough to

drive the observed orbital polarization and collective Jahn–Teller distortion. In order to be able to reproduce them, the orbital-dependent interaction terms must be included in the functional as is the case in the LDA + U method. It is possible to directly observe the orbital ordering in $KCuF_3$ by plotting the three-dimensional spin density obtained in the LDA + U calculation (figure 14). As there is only one hole in the d shell of the Cu^{2+} ion, this spin-density distribution gives the charge density of the holes. The picture agrees quite well with the orbital ordering of the alternating $x^2 - z^2$ and $y^2 - z^2$ Cu 3d orbitals. We notice that the charge distribution changes only very little under the influence of the lattice distortion, emphasizing that this ordering is in the first instance of an electronic origin.

As expected, the electronic properties come out essentially correct. The 'Koopman theorem' gap in the LDA + U band structure should give an order-of-magnitude estimate for the single-particle gap and was found to be similar to that in the cuprates (2 eV) [44]. Furthermore, the magnetic ordering is reproduced and to test the method more severely the magnetic exchange interactions were calculated as well. Using the Green function method to calculate the effective exchange interaction parameters as second derivatives of the ground-state energy with respect to the magnetic moment rotation angle [46] in combination with equations (4)–(9), one obtains

$$J_{ij} = \sum_{\{m\}} I^i_{mm'} \chi^{ij}_{mm'm''m'''} I^j_{m''m'''} \tag{47}$$

where the spin-dependent potentials I are expressed in terms of the potentials of equation (9),

$$I^i_{mm'} = V^{i\uparrow}_{mm'} - V^{i\downarrow}_{mm'} \tag{48}$$

while the effective inter-sublattice susceptibilities are defined in terms of the LDA + U eigenfunctions ψ as

$$\chi^{ij}_{mm'm''m'''} = \sum_{\boldsymbol{k}nn'} \frac{n_{n\boldsymbol{k}\uparrow} - n_{n'\boldsymbol{k}\downarrow}}{\epsilon_{n\boldsymbol{k}\uparrow} - \epsilon_{n'\boldsymbol{k}\downarrow}} \psi^{ilm*}_{n\boldsymbol{k}\uparrow} \psi^{jlm''}_{n\boldsymbol{k}\uparrow} \psi^{ilm'}_{n'\boldsymbol{k}\downarrow} \psi^{jlm'''*}_{n'\boldsymbol{k}\downarrow}. \tag{49}$$

It was found that the antiferromagnetic exchange in the CuF 'chains' amounts to $J_c = -20.7$ meV while the ferromagnetic exchange in the a–b planes is much smaller ($J_{ab} = 0.52$ meV), emphasizing the quasi-1D character of this $S = 1/2$ spin system. This compares quite well with the neutron scattering measurements, showing the Luttinger-liquid nature of the spin system, with the 1D exchange estimated to be $J_c = -17.5, -17.0$ meV and $J_{ab} = 0.17, 0.27$ meV [47]

6.2. Polarons in $La_{2-x}Sr_xCuO_4$ and $La_{2-x}Sr_xNiO_4$

The LDA + U method was designed to treat Mott–Hubbard insulators, but a real challenge is the problem of the theoretical description of the doped Mott insulator, the latter being the model for high-T_c superconductors based on copper oxides. One important question in this field is that of the strength of the polaronic effects in these compounds.

In order to answer this question Sr-doped (tetragonal) La_2CuO_4 was investigated [44]. The undoped system is quite well described by the LDA + U method and a 2×2 supercell ($La_{8-x}Sr_xCu_4O_{16}$) was used to investigate the (self-) localization effects. At first, the problem of the hole in the undistorted lattice was considered to address the magnetic relaxation effects. Subsequently the interaction of the hole with both in-plane and out-of-plane lattice distortions was investigated. These calculations were then repeated for $La_{2-x}Sr_xNiO_4$.

Except for the irrelevant La 4f states, the LDA + U electronic structure of undoped La_2CuO_4 looks very similar to that of $CaCuO_2$ (figure 6). According to these calculations,

La_2CuO_4 is a charge-transfer insulator [48]. The lowest unoccupied states are Cu $3d_{x^2-y^2}$, while the lowest occupied states are more O 2p-like. To see how well structural properties are handled, the frequency of the breathing-mode phonon were calculated. Using the frozen-phonon technique the calculated value was found to be $\omega_{BR} = 660$ cm^{-1}, quite close to the experimental value of 710 cm^{-1} [49].

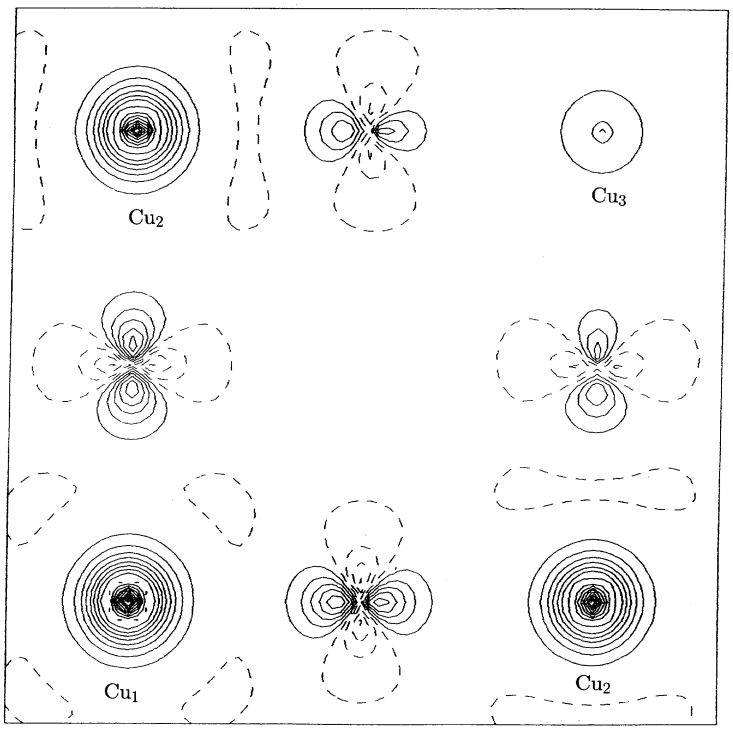

Figure 15. A contour map of the hole density distribution in the CuO_2 plane of La_2CuO_4 in the supercell LDA + U calculation. The central copper atom (Cu_1) is in the lower left-hand corner of the figure. The full lines correspond to the positive values and dashed lines to the negative values of the hole density.

It was found that the hole induces a parallel alignment of the moment of Cu_1 (the central Cu atom in supercell) with those of Cu_2 (nearest neighbours). This local ferromagnetic 'spin bag' in the antiferromagnetic background caused by the presence of a hole can be viewed as a mean-field analogue of the Zhang–Rice singlet [50]: the hole is mostly localized on the four oxygens surrounding the central Cu_1, having its spin antiparallel to that of Cu_1 (figure 15 and table 2). The hole-induced states produce the peak in the former gap region which is close (0.15 eV) to the top of the valence band.

In the study of lattice-polaronic effects two possible types of lattice deformation were investigated: (1) the four neighbouring in-plane O atoms were moved along the Cu–O bond axis toward Cu_1, where the hole is localized (the 'breathing polaron'), (2) the motion of the two apical O atoms (O_{ap}) along the Cu_1–O_{ap} bond axis was considered (the 'anti-JT polaron'). As a function of the breathing distortion it was found that *the energy is at minimum for a finite distortion, corresponding to a 2% contraction of the Cu_1–O_1 bond.* The total energy is lowered by an amount of 39 meV, and the energy is lower than that of

Table 2. The dependence of the total energy (meV) (δE) and the magnetic moments (in μ_B) on the displacement (x) of either in-plane ('breathing', BR) or apical oxygens ('Jahn–Teller', JT) towards the central transition metal ion (TM_1) in the supercell (TM_2 is the nearest and TM_3 the next-nearest TM_1 neighbour), in the case of 'doped' La_2CuO_4 (LCO) and La_2NiO_4 (LNO). (For JT the total energy δE is measured relative to the energy of BR.)

	x	δE	μ_{TM_1}	μ_{TM_2}	μ_{TM_3}
LCO	0%	0	−0.55	−0.59	0.72
	2% (BR)	−39	−0.43	−0.63	0.73
	11% (JT)	54	0.96	−0.64	0.73
LNO	0%	0	0.42	−1.58	1.67
	4% (BR)	−210	0.54	−1.58	1.67

the undistorted lattice up to a distortion of 4%. The calculated polaron binding energy is small compared to the estimates for its kinetic energy [51] and small-polaron effects are not expected.

It was found that the contraction of the Cu_1–O_{ap} bond increases the LDA + U total energy if the distortion is small. However, it was possible to find a local minimum in the total energy by allowing the additional hole to have $3z^2 - 1$ symmetry with respect to Cu_1, corresponding to a reduction of the Cu_1–O_{ap} bond length of 0.26 Å (11%), in remarkable agreement with the data of Egami *et al* [52]. *The total energy of the anti-JT polaron is only 54 meV higher than that of the fully relaxed breathing-mode polaron.*

The above calculations were repeated for Sr-doped La_2NiO_4. The undoped La_2NiO_4 was found to be a high-spin ($1.69\mu_B$) antiferromagnetic charge-transfer insulator with a p–d gap of 3.5 eV. The ground state is locally a $x^2 - y^2, 3z^2 - 1$ ($S = 1$) state, where the holes are rather strongly localized on Ni (10% O 2p admixture). Adding a hole to the supercell leads to an inhomogeneous state, which is qualitatively similar to the one in the cuprate. The additional hole has a large weight on the four in-plane O_1 atoms (nearest neighbours to Ni_1), although the 3d admixture has increased compared to the case of the cuprate. This state has $x^2 - y^2$ symmetry with respect to Ni_1 and the spin of the additional hole is antiparallel to that of Ni_1, i.e. the hole is low spin. The $x^2 - y^2$ spins do not compensate exactly on Ni_1 ($m_x = n_{x^2-y^2\uparrow} - n_{x^2-y^2\downarrow} = -0.30\mu_B$) and together with the larger polarization of the $3z^2 - 1$ hole ($0.70\mu_B$), give a net moment of $0.42\mu_B$ (table 2). The additional hole is nearly entirely localized on Ni_1 and O_1. Hence, *the magnetic confinement effects are much stronger in the nickelate than in the cuprate*. This is not surprising, considering the larger gap and moment in the former. Then the breathing-type lattice relaxation was studied, and *the stabilization energy of the breathing polaron was found to be 210 meV, five times larger than in the cuprate.* The total energy is at minimum if the Ni_1–O_1 bond is contracted by 4% (table 2). This large polaron binding energy could help to explain why doped nickelates are non-metallic in contrast to cuprates.

7. The metal–insulator transition

It is well known that mean-field approximation is too crude to be able to describe the metal–insulator transition in strongly correlated systems. However, there are a few cases where LDA + U calculations can be relevant to this problem. These are the cases of FeSi [53] and $LaCoO_3$ [54], both of them being non-magnetic insulators at low temperature and becoming metals with significant local magnetic moments at higher temperatures.

7.1. FeSi

FeSi displays an unusual crossover from a singlet semiconducting ground state with a narrow band gap to a metal with an enhanced spin susceptibility and a Curie–Weiss temperature dependence in the vicinity of room temperature [55]. Various theoretical models have been put forward to explain this behaviour starting with the very narrow-band description of Jaccarino *et al* [56]. Takahashi and Moriya (see [57]) proposed a nearly ferromagnetic semiconductor model which predicted thermally induced spin fluctuations which were subsequently confirmed experimentally [58]. Recently, models based on treating FeSi as a transition metal analogue of the Kondo insulators found in heavy-fermion rare-earth systems have been much discussed [59, 60].

The LDA electronic structure calculation by Mattheiss and Hamann [61] correctly accounts for the narrow-gap semiconducting ground state but more is required to explain the anomalous behaviour.

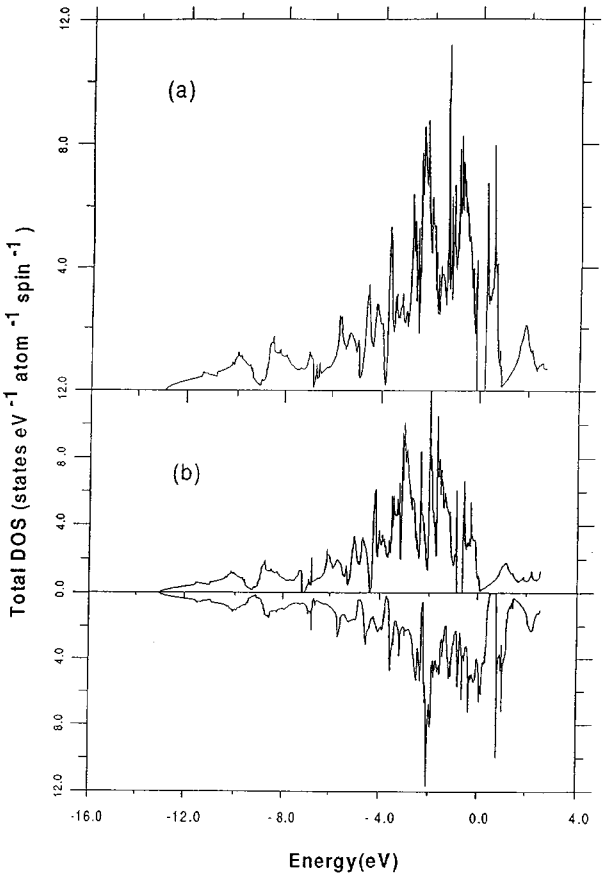

Figure 16. The density of states (DOS) for FeSi from LDA + U calculations. The chemical potential is the zero energy. (a) The non-magnetic state with $U = 0$; (b) majority- and minority-spin bands in a ferromagnetic state with a moment of $1\mu_B$ [53].

If one sets $U = 0$ then the potential correction (9) vanishes and the LDA + U method becomes equivalent to the standard LDA. In figure 16(a), the density of states (DOS)

obtained in the calculation with $U = 0$ is shown. It is quite close to the results of the previous LDA calculations [61]. The Stoner parameter, I, is not strong enough to produce a magnetic state and the only stable solution is non-magnetic. As one increases the value of U above the critical value, $U_c = 3.2$ eV, a stable magnetic solution appears with a magnetic moment on each Fe site, $\mu = 1\mu_B$ (figure 16(b)). The non-magnetic solution is still present and has a total energy of ≈0.3 eV/Fe lower than the magnetic one. With further increase of U the total energy of the magnetic solution decreases relative to the non-magnetic one and for $U > 4.6$ eV it is lower in energy and so becomes the ground state.

A so-called 'fixed-spin-moment' calculation was also performed where the total energy $E_g(\mu)$ is calculated as a function of the magnetic moment, μ, on each Fe site (figure 17). One can see that for $U < U_c$ there is only one local minimum in the curve corresponding to $\mu = 0$. Near $\mu \approx 1$ there is only a bend in the curve but no minimum. For $U = 3.4$ eV a second local minimum appears in the curve but it lies higher in energy than the zero-moment minimum. However, for $U = 5.4$ eV, the minimum corresponding to the magnetic solution is clearly lower than that for the non-magnetic one.

The existence of the second local minimum in $E_g(\mu)$ leads to a first-order transition in an external magnetic field. Although the magnetic moment ($\mu = 1\mu_B$/Fe) of the ferromagnetic state is insensitive to the choice of U, the critical field, B_c, that determines the transition is very sensitive to U. For example for the choice $U = 3.4$ eV corresponding to figure 17, B_c is very large ($\sim 10^3$ T), but for $U \geqslant 4.6$ eV, $B_c = 0$ and the magnetic solution is the most stable. It is clearly not possible to make an accurate *a priori* estimate of B_c. The authors [53] resorted to simpler model calculations guided by the *a priori* calculations which included the effect of finite temperature and then adjusted the model parameters to obtain agreement with the measured spin susceptibility $\chi(T)$ and specific heat $C_p(T)$. They obtained the critical temperature value $T_c = 280$ K and critical field $B_c = 170$ T.

7.2. $LaCoO_3$

Among the systems showing a semiconductor-to-metal transition, $LaCoO_3$ is especially interesting due to the fact that it also displays very unusual magnetic behaviour, often associated with low-spin–high-spin (LS–HS) transition [62]. Although a large number of investigations have been carried out since the early 1960s the character of the transition and the nature of the temperature dependence of the spin state is still unclear. For example, the temperature dependence of the magnetic susceptibility shows a strong maximum at around 90 K followed by a Curie–Weiss-like decrease at higher temperatures [63] which was interpreted by the authors as a LS–HS transition. The semiconductor–metal-like transition occurs in the range 400–600 K, well above this transition.

The electronic structure of $LaCoO_3$ was studied [54] in the LDA + U approach. In contrast to the results from the standard LDA there were found several stable solutions corresponding to different local minima of the LDA + U functional. The non-magnetic insulating low-spin state (the d-shell configuration of the Co ion is $t_{2g}^6 e_g^0$) is a ground state, in agreement with the experiment. The unexpected result was that while the high-spin state (configuration $t_{2g}^4 e_g^2$) lies rather high in energy, two other orbitally polarized magnetic solutions (configuration $t_{2g}^5 e_g^1$) corresponding to intermediate-spin (IS) states (one of them is a gapless semiconductor and the other is a metal) have total-energy values only slightly higher than that of the LS ground state (for crystal structure parameters corresponding to the temperature 4 K). The total-energy difference between the LS and IS states is very sensitive to the lattice constant. With increasing lattice constant the energy of the IS solution becomes smaller than the total energy of the LS solution thus giving the IS solution as a ground

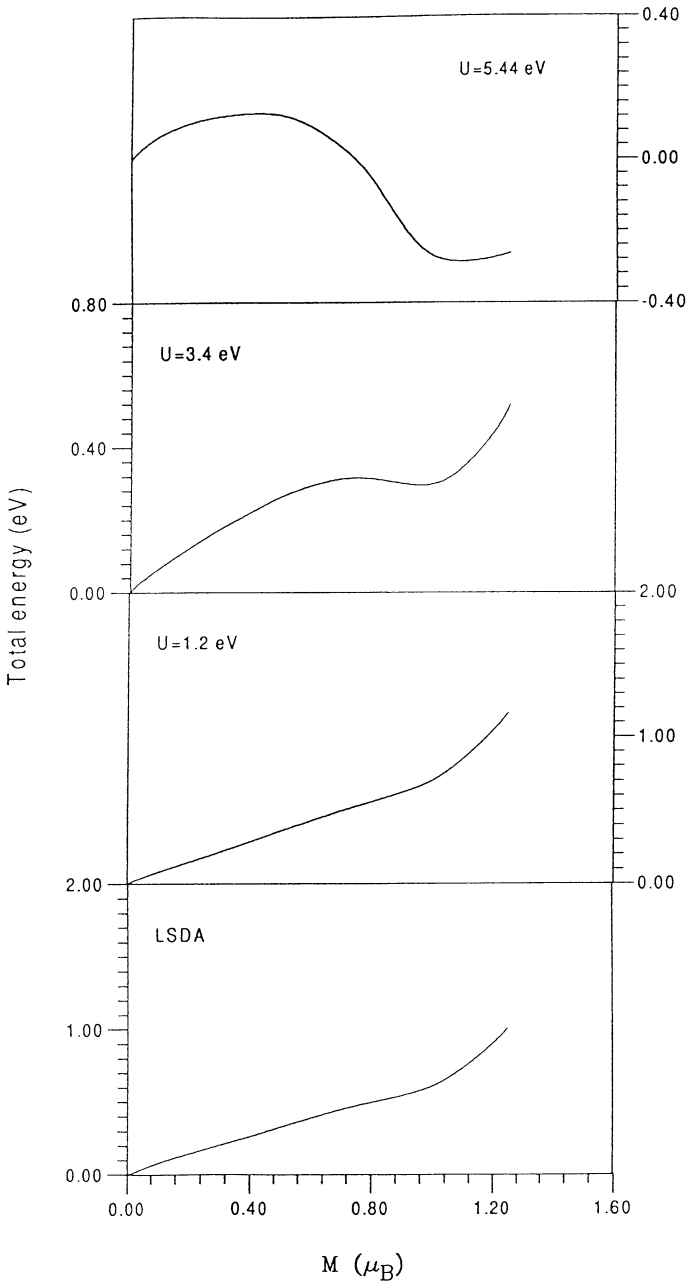

Figure 17. The total energy of FeSi as a function of the spin moment M (μ_B/Fe) with various values of U [53].

state. This crossover occurs at the lattice constant corresponding to $\simeq$150 K. The authors of [54] suggested the following interpretation of the transition in $LaCoO_3$. According to their scheme, with increasing temperature, at first a transition from a LS (non-magnetic) insulating ground state to a state with an IS (configuration $t_{2g}^5 e_g^1$) occurs. Due to the strong

Jahn–Teller nature of this configuration, this state may develop an orbital ordering. The orbitally ordered state turns out to be non-metallic (actually a nearly zero-gap semiconductor) in the LDA+U calculations. With the further increase of the temperature the orbital ordering may be gradually destroyed which can explain the transition to a metallic state observed in $LaCoO_3$ at 400–600 K.

8. A charge-ordered insulator: Fe_3O_4

Magnetite Fe_3O_4 is a mixed-valence 3d transition metal compound. It crystallizes in an inverted cubic spinel structure in which the tetrahedral A sites contain one third of the Fe ions as Fe^{3+}, while the octahedral B sites contain the remaining Fe ions, with equal numbers of Fe^{3+} and Fe^{3+} ions in B1 and B2 sites, respectively. Below 860 K, magnetite is ferrimagnetic with A-site magnetic moments aligned antiparallel to the B-site moments. At $T_V = 122$ K Fe_3O_4 undergoes a first-order phase transition, the so-called Verwey transition (see [64]), in which dc conductivity abruptly increases by two orders of magnitude on heating through T_V. Verwey interpreted the transition as an order–disorder transformation of Fe ions on the B sites. Indeed, studies by electron and neutron diffraction, and nuclear magnetic resonance [65] show that below T_V the B1 and B2 sites are structurally distinguishable in a distorted crystal structure. Photoemission measurements clearly show a gap of $\simeq$0.14 eV in the spectra [66]. However, a band-structure calculation using local spin-density approximation (LSDA) [67] gave only a metallic solution without charge ordering with a partially filled band (containing one electron per two B sites) originated from t_{2g} spin-down 3d orbitals of Fe ions in octahedral B sites.

The problem of the charge ordering cannot be treated using the standard LSDA. The reason for this is a spurious self-interaction which is present in the LSDA. In contrast to the Hartree–Fock approximation where self-interaction is explicitly excluded for every orbital, in the LSDA it is cancelled only in the total-energy integrals but not in one-electron potentials which are orbital independent. The spurious self-interaction present in the LSDA leads to an increase in the Coulomb interaction when the distribution of the electron charge deviates from the uniform one. This effect can be illustrated in the following way. If one neglects inter-site Coulomb interaction then the electron under consideration feels the same potential on all sites independently of the occupancy of the particular site, as it does not interact with itself. However, as the LSDA potential is a functional of the electron density only, then, increasing the electron density on one site and decreasing it on another one, with a development of charge ordering, will lead to an increase of the potential on the first site and a decrease on the second one. As a result, in the self-consistency loops, the charge distribution will return to the uniform density.

In order to cure this deficiency, it is necessary to remove spurious self-interaction. Formally the LDA + U method does it but this method was constructed for Mott insulators, and for systems with a charge ordering it must be modified by taking into account inter-site Coulomb interaction. In order to do this one must map the dependence of the Coulomb interaction energy onto the number of t_{2g} electrons in the LSDA of a model with on-site and inter-site terms, and then explicitly exclude the self-interaction on-site term [68].

If one defines n_i as a sum of the occupancies of t_{2g} orbitals ($n_{xy} + n_{xz} + n_{yz}$) for the minority-spin direction on B site i then the model which imitates the LSDA is

$$E[n_i] = \sum_i \left\{ \frac{1}{2} U n_i (n_i - 1) + V \sum_j n_i n_j \right\}. \tag{50}$$

(The index j numbers the neighbours of the site i.) In order to compute the value of

the parameters U and V one must perform a constrained calculation for the two types of charge ordering where occupancies n_i on different sites are varied with the total number of t_{2g} electrons conserved. As a first type of charge ordering, the order suggested by Verwey (see [64]) was chosen. It can be described as a lattice built from the neutral tetrahedra where every tetrahedron contains two atoms from the B1 sublattice and two atoms from the B2 sublattice. The second type of charge ordering corresponds to charged tetrahedra where one of them contains only B1-type and another only B2-type entities.

Having determined the parameters U and V one can define now a new functional without a self-interaction by subtracting a $\frac{1}{2}Un_i(n_i-1)$ term from the LSDA functional. The real on-site Coulomb interaction energy is small due to the small probability of meeting two t_{2g} electrons on the same site but it is nevertheless non-zero and it was taken into account by adding the corresponding term in the Hartree–Fock approximation:

$$E = E_{LSDA} - \frac{1}{2}\sum_i \left\{ Un_i(n_i-1) - \sum_{m,m'\neq m} Un_{i,m}n_{i,m'} \right\} \tag{51}$$

(here m, m' denotes different t_{2g} orbitals for spin-down electrons of Fe ions on octahedral B sites). The corresponding orbital-dependent potential $V_{i,m}$ is given by the variation of the new functional (6) with respect to the occupancy of the particular t_{2g} orbital $n_{i,m}$:

$$V_{i,m} = V_i^{LSDA} + U\left(\frac{1}{2} - n_{i,m}\right).$$

Constrained calculations with two types of charge ordering gave the following parameters: $U = 4.51$ eV and $V = 0.18$ eV.

Electronic structure calculations for the functional given in equation (51) were performed for the Verwey type of charge ordering. In contrast to the LSDA, where the stable solution is a metal with a uniform distribution of the t_{2g} spin-down electrons on the octahedral sites, the self-interaction-corrected functional (51) gave a charge-ordered insulator with an energy gap of 0.34 eV (the experimental value is 0.14 eV [66]).

According to the ionic model, charge ordering implies Fe^{3+} and Fe^{2+} ions on octahedral-site sublattices B1 and B2 with configurations d^5 ($t_{2g\uparrow}^3 e_{g\uparrow}^2$) and d^6 ($t_{2g\uparrow}^3 e_{g\uparrow}^2 t_{2g\downarrow}^1$) respectively. In the actual calculations due to the strong covalency effects the numbers of d electrons in the atomic spheres were 5.91 and 6.23 with the charge difference 0.32 instead of the pure ionic value of 1.0 (however, the difference in the occupancy of the $t_{2g\downarrow}$ orbital for two sublattices is larger: 0.70).

In figure 18, the densities of states (DOSs) for Fe_3O_4 obtained in standard LSDA calculations are presented and in figure 19 the DOS calculated with the use of the functional in equation (51) is shown. For the LSDA one can see an oxygen band between -8 eV and -4 eV and above it (for both spin-up and spin-down DOSs) four bands of Fe 3d origin. For spin-up states the sequence is t_{2g} and e_g bands of iron in octahedral B sites and above them e_g and t_{2g} bands of iron in tetrahedral A sites. For spin-down states the order of the octahedral and tetrahedral sites bands is reversed so the first two d bands are e_g and t_{2g} bands of iron in tetrahedral sites (A) and above them are t_{2g} and e_g bands of iron in octahedral sites (B) with the Fermi energy lying in the t_{2g} band.

In the charge-ordered state the partially filled t_{2g} spin-down band of the octahedral (B) ions is split into three parts (figure 19): just below the Fermi energy is the subband corresponding to the occupied t_{2g} orbital of the B2(Fe^{2+}) sublattice, then immediately above the Fermi energy is the t_{2g} band of the B1(Fe^{3+}) sublattice and above it the band formed by the empty orbitals of B2(Fe^{2+}) ions and empty e_g bands of octahedral (B1, B2) ions.

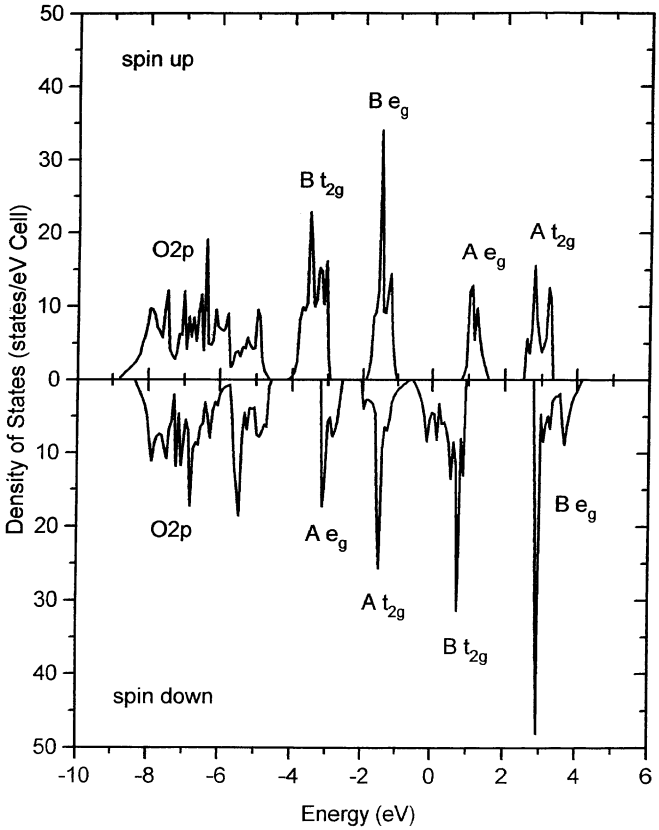

Figure 18. The density of states for Fe_3O_4 in the LSDA calculation. A: tetrahedrally coordinated Fe ions; B: octahedral Fe ions [68].

This result shows that, after subtracting the spurious self-interaction present in the LSDA, it is indeed possible to obtain an insulating charge-ordered solution for Fe_3O_4. However, what about the metal–insulator transition—can this method describe it? Knowing the value of the inter-site Coulomb interaction parameter V it is possible to estimate the change in the potential acting on the t_{2g} electrons in going from Verwey-type charge order to the completely disordered state. The difference between the electrostatic potentials for the two sublattices in Verwey-type charge order is equal to $\delta V = 4V\,\delta n_{t_{2g}}$. The calculation of [68] gave $V = 0.18$ eV and $\delta n_{t_{2g}} = 0.70$ which gives the result $\delta V = 0.50$ eV and that is definitely larger than the calculated energy gap value, 0.34 eV. That means that completely destroying the charge order would close the energy gap and lead to the metallic state.

9. Beyond the mean-field approximation: spectral properties and quasiparticle bands

In spite of its many successes the LDA + U method has obvious limitations as a one-electron method with a single Slater determinant as a trial function. It is well known that, for example, spectra of the transition metal compounds could only be described in the configuration interaction (CI) approximation with a trial function which is a linear combination of the Slater determinants [14, 15].

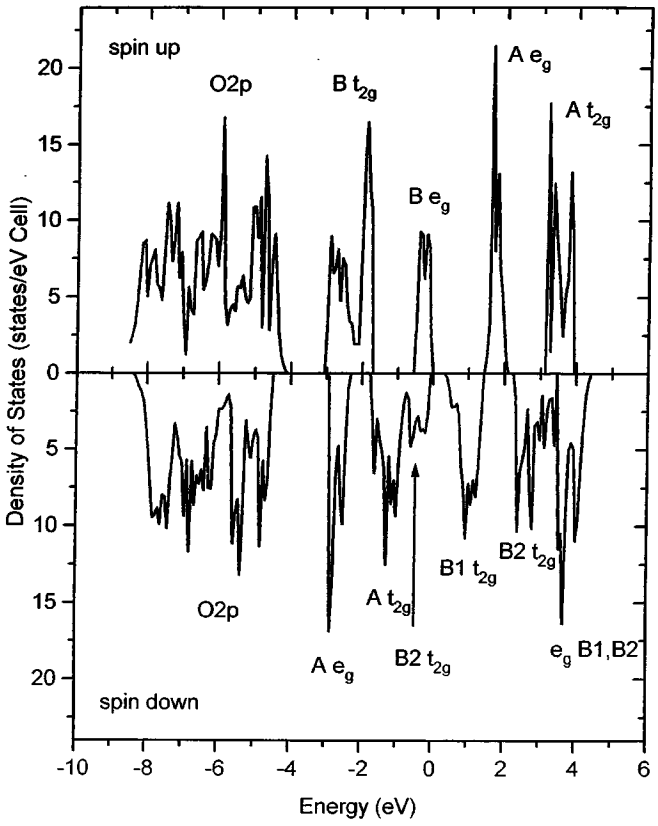

Figure 19. The density of states for Fe_3O_4 in the LDA + U calculation. A: tetrahedrally coordinated Fe ions; B: octahedral Fe ions (B1 corresponds to Fe^{3+} and B2 to Fe^{2+} ions) [68].

The LDA + U method can give all of the parameters needed for such calculations because the diagonal matrix elements for every single Slater determinant can be calculated in the framework of the LDA + U theory and the off-diagonal matrix elements can be expressed through the one-electron parameters. The following [69] is the realization of this idea for the case of NiO, but the procedure is general and could be applied to any material.

The ground state of NiO (with N particles) in the Anderson impurity model is

$$\Psi_{GS}^{N} = \alpha_0 |\mathrm{d}^8\rangle + \beta_0 |\mathrm{d}^9 L\rangle \tag{52}$$

where L is a hole in the ligand states (the oxygen continuum) and the high-energy $|\mathrm{d}^{10}L^2\rangle$ configuration is neglected. The final states of the removal spectrum (with $N-1$ particles) are (neglecting the $|\mathrm{d}^9L^2\rangle$ configuration)

$$\Psi_{m}^{N-1} = \alpha_m |\mathrm{d}^7\rangle + \beta_m |\mathrm{d}^8 L\rangle. \tag{53}$$

The one-electron-removal Green function is

$$G(\omega) = \sum_m \frac{A_m}{\omega - E_m^{N-1} + E_{GS}^{N} + \mathrm{i}\eta}. \tag{54}$$

The pole strengths A_m are the squares of the overlaps between the eigenstates Ψ_m^{N-1} and the state obtained by suddenly removing an electron from the ground state Ψ_{GS}^{N-1}. The form

of the function Ψ_{GS}^{N-1} depends on from which orbital an electron will be removed—from Ni 3d or from O 2p. In the first case

$$\Psi_{GS,d}^{N-1} = \alpha_0|\mathrm{d}^7\rangle + \beta_0|\mathrm{d}^8\underline{L}\rangle. \tag{55}$$

In the second case

$$\Psi_{GS,p}^{N-1} = \alpha_0|\mathrm{d}^8\underline{L}\rangle + \beta_0|\mathrm{d}^9\underline{L}^2\rangle. \tag{56}$$

The corresponding pole strengths are

$$A_m^d = |\langle\Psi_{GS,d}^{N-1}|\Psi_m^{N-1}\rangle|^2 = |\alpha_0\alpha_m + \beta_0\beta_m|^2 \tag{57}$$

$$A_m^p = |\langle\Psi_{GS,p}^{N-1}|\Psi_m^{N-1}\rangle|^2 = |\alpha_0\beta_m|^2. \tag{58}$$

The corresponding one-electron Green's functions for removal of d and p electrons are

$$G_d(\omega) = \alpha_0^2 G_{dd} + \alpha_0\beta_0(G_{dp} + G_{pd}) + \beta_0^2 G_{pp} \tag{59}$$

$$G_p(\omega) = \alpha_0^2 G_{pp} \tag{60}$$

where

$$G_{\alpha\beta} = \sum_m \frac{\alpha_m\beta_m^*}{\omega - E_m^{N-1} + E_{GS}^N + \mathrm{i}\eta}. \tag{61}$$

Let us consider first the d-removal spectrum. The final state with three d holes $|\mathrm{d}^7\rangle$ can have any of three symmetries: ^{2}E (the $\mathrm{e}_{\mathrm{g}\uparrow}^1\mathrm{e}_{\mathrm{g}\downarrow}^2$ hole configuration), $^4\mathrm{T}_1$ ($\mathrm{t}_{2\mathrm{g}\downarrow}^1\mathrm{e}_{\mathrm{g}\downarrow}^2$) and $^2\mathrm{T}_1$ ($\mathrm{t}_{2\mathrm{g}\uparrow}^1\mathrm{e}_{\mathrm{g}\downarrow}^2$). They can mix with the configurations $|\mathrm{d}^8\underline{L}\rangle$ of the corresponding symmetries. The non-zero off-diagonal matrix elements can be expressed through the one-electron hopping parameters (properly given in LDA or LDA + U calculations) and the corresponding coefficients are tabulated in [70, 14].

How do we calculate the diagonal matrix elements, for example $\langle\mathrm{e}^3|\mathrm{e}^3\rangle$ and $\langle\mathrm{e}^2(^3\mathrm{A}_2)\underline{L}_e|\mathrm{e}^2(^3\mathrm{A}_2)\underline{L}_e\rangle$? If the energy of the ground state of the $|\mathrm{d}^8\rangle$ configuration ($|\mathrm{e}^2(^3\mathrm{A}_2)\rangle$) is zero then the former is the removal energy of the $\mathrm{e}_{\mathrm{g}\uparrow}$ electron and the latter is the removal energy of the ligand (oxygen 2p) electron. In the LDA + U formalism the one-electron energies of the occupied states have the meaning of the removal energies [12] so one can use the results of the self-consistent LDA + U calculation for the calculation of the diagonal matrix elements of the many-electron Hamiltonian. If the particular $|\mathrm{d}^8\underline{L}\rangle$ state has a d^8 configuration not in the ground state $^3\mathrm{A}_2$ (for example $|\mathrm{e}^2(^1\mathrm{E})\underline{L}_e\rangle$) then the diagonal matrix element will be the energy of $\underline{L}_e$ minus the energy difference ($E(^1\mathrm{E}) - E(^3\mathrm{A}_2)$).

In practice, the calculations were performed in the following way. At first the many-electron Hamiltonian matrix, whose eigenfunctions are Ψ_m^{N-1}, equation (53), was constructed from the parts of the one-electron Hamiltonian, and then the Green functions (61) were calculated. Let us illustrate this for ^{2}E symmetry.

In the one-electron Hamiltonian matrix there is one block describing continuum states (O 2p), two rows (columns) for d orbitals of e_g symmetry and three rows (columns) for $\mathrm{t}_{2\mathrm{g}}$. In the many-electron Hamiltonian matrix for ^{2}E symmetry there are three blocks for continuum states (describing three types of ligand hole in the final states $|\mathrm{d}^8\underline{L}\rangle$) with the shifts of the diagonal elements of these blocks if the corresponding d^8 configuration is not in the ground state $^3\mathrm{A}_2$. There is also one row (column) for $|\mathrm{d}^7\rangle$ (e^3) configuration with the diagonal matrix element equal to the energy of the $\mathrm{e}_{\mathrm{g}\uparrow}$ orbital in LDA + U calculations and with the off-diagonal matrix elements according to [70, 14].

To perform impurity calculations for NiO with only one d shell in an oxygen continuum, we use the following procedure. We first push up the d orbitals by adding a potential acting only on them:

$$H_0 = H_{LDA+U} + \sum_i |d_i\rangle \Delta \langle d_i|. \tag{62}$$

Δ is a constant and i labels the site. The valence band is then mainly formed by the Ni 4s, 4p and O 2s, 2p orbitals with a small but non-zero hybridization with the Ni d decaying as $\sim 1/\Delta$. Using the Hamiltonian H_0 we calculate the Green function G^0_{dd} which has a small imaginary part around the valence band due to the small hybridization. The impurity Green function G_{dd} is then defined to be the one corresponding to the following Hamiltonian:

$$H = H_0 - |d_0\rangle \Delta \langle d_0| \tag{63}$$

i.e. at the origin where the impurity is located, the d orbital is at its original position but at any other site it is high up in energy. Consequently, this Green function contains the hybridization with the oxygen continuum through H_0. The impurity Green function can be calculated from the Dyson equation:

$$G = G_0 + G_0 \, \Delta V \, G \tag{64}$$

where for the d orbital, $V = |d_0\rangle \Delta \langle d_0|$ giving well known formulae [71]

$$G_{dd} = \frac{G^0_{dd}}{1 - \Delta G^0_{dd}} \tag{65}$$

$$G_{dp} = \frac{G^0_{dp}}{1 - \Delta G^0_{dd}} \tag{66}$$

$$G_{pp} = \frac{G^0_{pd} \Delta G^0_{dp}}{1 - \Delta G^0_{dd}} + G^0_{pp}. \tag{67}$$

Δ is the upward energy shift of the d orbitals for calculating Green's functions G^0:

$$G^0_{ij}(\omega) = \int \mathrm{d}\boldsymbol{k} \sum_n \frac{c^n_i(\boldsymbol{k}) c^{n*}_j(\boldsymbol{k})}{\omega - E^n(\boldsymbol{k}) + \mathrm{i}\eta}. \tag{68}$$

The integration is over the Brillouin zone and $c^n_i(\boldsymbol{k})$, $E^n(\boldsymbol{k})$ are eigenvectors and eigenvalues of the band-structure calculation with the new Hamiltonian matrix.

Equations (65)–(68) and (59) were used to calculate the one-electron Green's function for the removal of a d electron, $G_d(\omega)$. (The α_0 and β_0 were extracted from the ground-state self-consistent LDA + U calculation: $\alpha_0^2 \approx 0.9$ and $\beta_0^2 \approx 0.1$.)

The total d-removal theoretical spectrum was calculated from the imaginary part of the $G_d(\omega)$ broadened by 0.5 eV (the summation over the three symmetries of the final state (^{2}E, ^{2}T and ^{4}T) with appropriate weights was performed). In figure 20 this spectrum is plotted together with experimental XPS for NiO. One can see that two major features of the experimental spectra—the main line at the top of the valence band and a satellite at $\approx$8 eV lower in energy with smaller intensity—are well reproduced not only in energy separation but also in intensity ratio.

By using expression (60) one can calculate the oxygen p-removal spectra. In figure 21 they are plotted together with the experimental O Kα x-ray emission spectrum (XES) of NiO. The impurity approximation, which was used in our calculations, is a d-ion-centred approach and not so well suited for the oxygen states, but it reproduced two major features of the experimental spectrum: the main peak of the oxygen bands and the high-energy

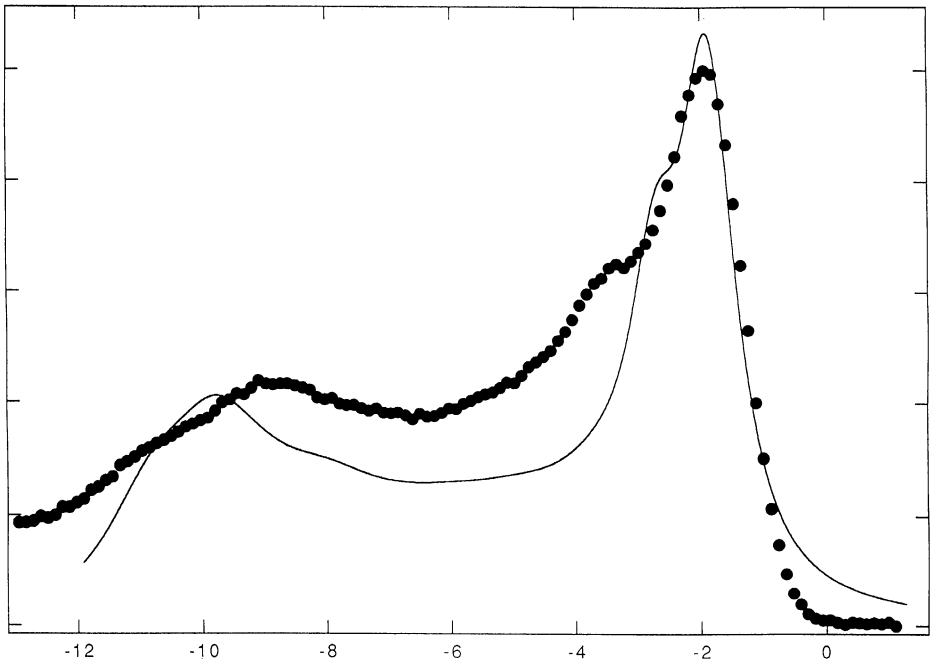

Figure 20. The calculated (Green function LDA + U) d-emission spectrum (line) and experimental XPS for NiO (dots) [69].

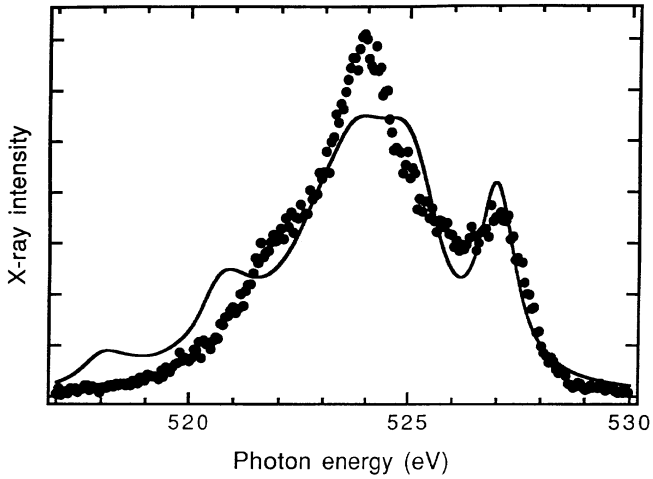

Figure 21. The calculated (Green function LDA + U) p-emission spectrum for NiO (line) and experimental O Kα x-ray emission spectrum for NiO (dots) [69].

shoulder corresponding to the admixture of the oxygen states to the main line of the d-removal spectrum.

While XPS gives the distribution of the d states and O Kα XES that of the p states, the photoemission spectrum taken at a photon energy of 40.8 eV, shown in figure 22,

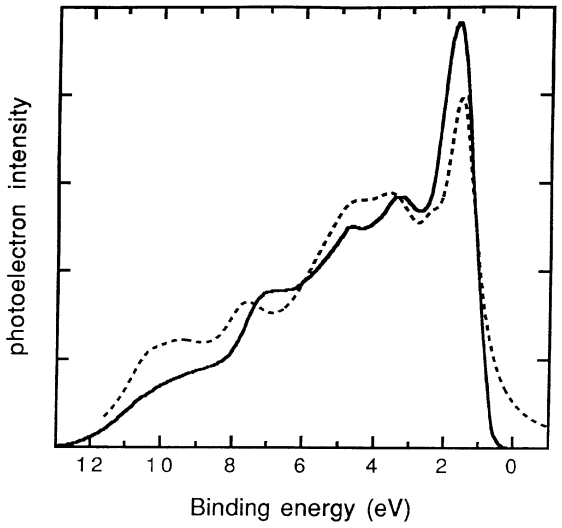

Figure 22. The calculated (Green function LDA + U) photoemission spectrum with equal weights of Ni 3d and O 2p states (dashed line) compared to the experimental He II UPS (solid line) [69].

corresponds to nearly equal cross-sections of Ni 3d and O 2p states. Good agreement with the theoretical spectrum, obtained by adding the Ni 3d- and the O 2p-removal spectra, proves that our calculation gives not only the main line and satellites of d origin but also the relative position of the oxygen bands.

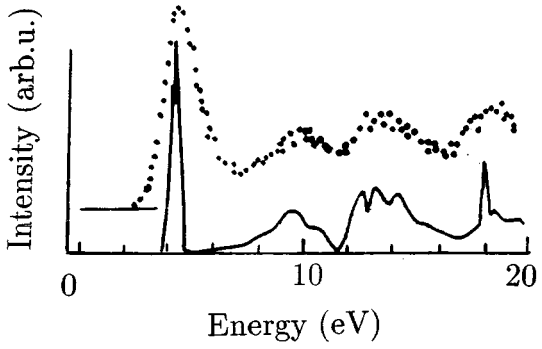

Figure 23. The experimental (dots) and the calculated (solid line) BIS (bremsstrahlung isochromat spectrum) for NiO [12].

The final state of the addition spectrum for NiO has only one d hole and the corresponding wave function could be chosen as a single Slater determinant. Hence the straightforward LDA + U calculation of the density of states for unoccupied bands must be compared with 'bremsstrahlung isochromat spectra' (BIS). Such a comparison is presented in figure 23 and it shows quite good agreement.

One of the most promising ways of going beyond mean-field LDA + U approximation is a 'dynamical mean-field' approach, [72] which takes into account full local quantum

fluctuations on d (f) sites in the impurity-like model. A non-trivial frequency dependence of the self-energy could describe the Mott metal–insulator transition in transition metal oxides, such as V_2O_3, for a different temperature and interaction strength U/t. In this case only spatial fluctuations between different d (f) sites are frozen and it could be a perfect approximation for heavy-fermion systems. If the Hubbard parameter U is smaller than the band width, it is possible to use one of the 'standard conserving approximations'—fluctuation exchange approximation (FLEX) [73] and investigate the general $\boldsymbol{q}$- and ω-dependence of a self-energy. We briefly illustrate this approach to the problem of quasiparticle band structure for bi-layer superconducting cuprates, such as $YBa_2Cu_3O_7$.

In this case the total Green function matrix in the orbital and spin space determined through the self-consistent solution of FLEX equations is

$$\begin{aligned} G^{-1}(\boldsymbol{k},\omega_n) &= G_0^{-1}(\boldsymbol{k},\omega_n) - \Sigma(\boldsymbol{k},\omega_n) \\ \Sigma(\boldsymbol{k},\omega_n) &= \frac{T}{N}\sum_{\boldsymbol{q},\omega_m} V(\boldsymbol{q},\omega_m)G(\boldsymbol{k}-\boldsymbol{q},\omega_n-\omega_m) \end{aligned} \tag{69}$$

where N is a total number of momentum $\boldsymbol{k}$-points, $\omega_n = (2n+1)\pi T$ are the fermion Matsubara frequencies with n an integer and T the system temperature. The spin-fluctuation contribution to the effective interaction matrix V in the paramagnetic state

$$V^{sf}(\boldsymbol{q},\omega_m) = (3/2)U\chi(\boldsymbol{q},\omega_m)[(1-U\chi(\boldsymbol{q},\omega_m))^{-1}-1]U$$

is defined through the full particle–hole susceptibilities:

$$\chi^{ph}_{mm'm''m'''}(\boldsymbol{q},\omega_m) = -\frac{T}{N}\sum_{\boldsymbol{q},\omega_m} G_{mm''}(\boldsymbol{k},\omega_n)G_{m'm'''}(\boldsymbol{k}+\boldsymbol{q},\omega_n+\omega_m). \tag{70}$$

Here the U-matrix corresponds to the antisymmetrized Coulomb interaction from equation (10), namely $U_{mm'm''m'''} = \langle mm''|V_{ee}|m'm'''\rangle - \langle mm''|V_{ee}|m'''m'\rangle$.

For $YBa_2Cu_3O_7$ we include in the consideration only two antibonding Cu $d_{x^2-y^2}$–O p_x, p_y LDA bands which only cross the Fermi level for this bi-layer CuO_2 system [74]. The band width is approximately 4 eV, and the effective Hubbard parameter is 3 eV. The latter number takes into account the 65%-weight Cu $d_{x^2-y^2}$ orbital in these antibonding bands and the LDA screened electron–electron interaction parameter for the Cu d orbital in cuprate of about 7–8 eV. We solve the non-linear integral FLEX equations using the fast Fourier transform method on the discrete mesh of 64×64 momenta in the two-dimensional Brillouin zone and 700–800 Matsubara frequencies with the cut-off of 20–30 eV in the energy (which corresponds to the temperature range of 80–200 K). Analytical continuation on the real axes was done by Padé approximation.

The resulting quasiparticle (QP) bands which correspond to the maxima in the spectral functions ($A(\boldsymbol{k},\omega) = -(1/\pi)\mathrm{Im}\,G(\boldsymbol{k},\omega)$) are presented on figure 24, in comparison with the bare LDA bands. Due to the large spin fluctuation for the $\boldsymbol{q} = (\pi,\pi)$ point in the two-dimensional Brillouin zone (BZ), there is a large renormalization of the bi-layer splitting near the X point. While the Fermi-level-crossing points are nearly the same for LDA bands and QP bands by the Luttinger theorem, the bonding (b) and antibonding (a) QP bands are 'pinned' to the Fermi level in a large portion of the BZ, forming so-called 'extended van Hove singularities'. The important property of such QP band structures of HTC compounds is the 'vanishing' of the bi-layer splitting in agreement with the recent angle-resolved photoemission study [75]

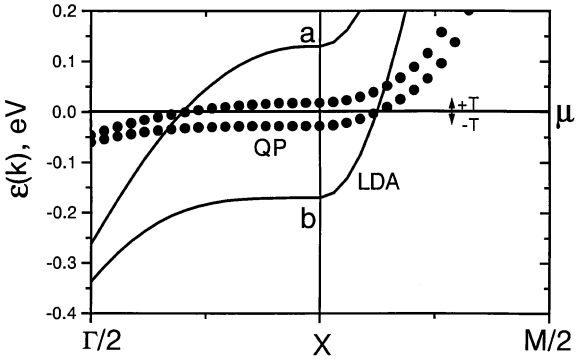

Figure 24. LDA and QP bands near the X point for bi-layer cuprates. Arrows indicate the temperature scale ($T = 150$ K), $\Gamma/2 \equiv (\pi/2, 0)$, $M/2 \equiv (\pi, \pi/2)$.

10. Conclusion

The LDA + U method was proved to be a very efficient and reliable tool in calculating the electronic structure of systems where the Coulomb interaction is strong enough to cause localization of the electrons. It works not only for nearly core-like 4f orbitals of rare-earth ions, where the separation of the electronic states in the subspaces of the infinitely slow localized orbitals and infinitely fast itinerant ones is valid, but also for such systems as transition metal oxides, where 3d orbitals hybridize quite strongly with oxygen 2p orbitals. In spite of the fact that the LDA + U method is a mean-field approximation which is in general insufficient for the description of the metal–insulator transition and strongly correlated metals, in some cases, such as the metal–insulator transitions in FeSi and $LaCoO_3$, LDA + U calculations gave valuable information by giving insight into the nature of these transitions. The main advantage of the LDA + U method over model approaches is its 'first-principles' nature with a complete absence of adjustable parameters. Another asset is its fully preserved ability from LDA-based methods to address the intricate interplay of the electronic and lattice degrees of freedom by computing the total energy as a function of lattice distortions. When the localized nature of the electronic states with Coulomb interaction between them is properly taken into account, this ability allows one to describe such effects as polaron formation and orbital polarization. As the spin and charge densities of the electrons are calculated self-consistently in the LDA + U method, the resulting diagonal and off-diagonal matrix elements of one-electron Hamiltonians could be used in more complicated calculations where many-electron effects are treated beyond the mean-field approximation.

Acknowledgment

This work was in part supported by the Russian Foundation for Basic Research (RFFI grant 96-02-16167).

References

[1] Hohenberg P and Kohn W 1964 *Phys. Rev.* **136** B864
Kohn W and Sham L J 1965 *Phys. Rev.* **140** A1133

[2] Svane A and Gunnarsson O 1990 *Phys. Rev. Lett.* **65** 1148
[3] Massida S, Posternak M and Baldereschi A 1993 *Phys. Rev.* B **48** 5058
[4] Gunnarsson O, Andersen O K, Jepsen O and Zaanen J 1989 *Phys. Rev.* B **39** 1708
[5] Anisimov V I and Gunnarsson O 1991 *Phys. Rev.* B **43** 7570
[6] Hedin L 1965 *Phys. Rev.* **139** A796
[7] Hedin L and Lundqvist S 1969 *Solid State Physics* vol 23, ed H Ehrenreich, F Seitz and D Turnbull (New York: Academic) p 1
[8] Aryasetiawan F 1992 *Phys. Rev.* B **46** 13 051
[9] Godby R W, Schlüter M and Sham L J 1988 *Phys. Rev.* B **37** 10 159
[10] Aryasetiawan F and Gunnarsson O 1995 *Phys. Rev. Lett.* **74** 3221
[11] Anisimov V I, Zaanen J and Andersen O K 1991 *Phys. Rev.* B **44** 943
[12] Anisimov V I, Solovyev I V, Korotin M A, Czyzyk M T and Sawatzky G A 1993 *Phys. Rev.* B **48** 16 929
[13] Lichtenstein A I, Zaanen J and Anisimov V I 1995 *Phys. Rev.* B **52** R5467
[14] Fujimori A and Minami F 1984 *Phys. Rev.* B **30** 957
[15] van Elp J, Potze R H, Eskes H, Berger R and Sawatzky G A 1991 *Phys. Rev.* B **44** 1530
[16] Anderson P W 1961 *Phys. Rev.* **124** 41
[17] Judd B R 1963 *Operator Techniques in Atomic Spectroscopy* (New York: McGraw-Hill)
[18] de Groot F M F, Fuggle J C, Thole B T and Sawatzky G A 1990 *Phys. Rev.* B **42** 5459
[19] Andersen O K 1975 *Phys. Rev.* B **12** 3060
[20] Harmon B N, Antropov V P, Lichtenstein A I, Solovyev I V and Anisimov V I 1995 *J. Phys. Chem. Solids* **56** 1521
[21] Riegel D, Gross K D and Luszik-Bhadra M 1987 *Phys. Rev. Lett.* **59** 1244
Gross K D, Riegel D and Zeller R 1989 *Phys. Rev. Lett.* **63** 1176
Gross K D and Riegel D 1988 *Phys. Rev. Lett.* **61** 1249
[22] Anisimov V I and Dederichs P H 1992 *Solid State Commun.* **84** 241
[23] Solovyev I V, Dederichs P H and Anisimov V I 1994 *Phys. Rev.* B **50** 16 861
[24] Fisher P, Lebech B, Meier G, Rainford B D and Vogt O 1978 *J. Phys. C: Solid State Phys.* **11** 345
Meier G, Fisher P, Haly W, Lebech B, Rainford B D and Vogt O 1978 *J. Phys. C: Solid State Phys.* **11** 1173
[25] Norman M R and Koelling D D 1986 *Phys. Rev.* B **33** 6730
[26] Kasuya T, Sakai O, Tanaka J, Kitazawa H and Suzuki T 1987 *J. Magn. Magn. Mater.* **63–64** 9
[27] Lichtenstein A I, Antropov V P and Harmon B N 1994 *Phys. Rev.* B **49** 10 770
[28] Fehrenbacher R and Rice T M 1993 *Phys. Rev. Lett.* **70** 3471
[29] Lichtenstein A I and Mazin I I 1995 *Phys. Rev. Lett.* **74** 1000
[30] Sawatzky G A and Allen J W 1984 *Phys. Rev. Lett.* **53** 2239
[31] de Groot F M F, Grioni M, Fuggle J C, Ghijsen J, Sawatzky G A and Petersen H 1989 *Phys. Rev.* B **40** 5715
[32] Haas K C 1989 *Solid State Physics* vol 42, ed C H Ehrenreich and D Turnbull (New York: Academic)
[33] Zaanen J 1989 *Proc. Int. Symp. on High-T_c Superconductivity (Jaipur, India)* ed K B Karg (New Delhi: Oxford University Press)
[34] Gunnarsson O, Jepsen O and Shen Z-X 1990 *Phys. Rev.* B **42** 8707
[35] Fuggle J C, Weiss P J W, Schoorl R, Sawatzky G A, Fink J, Nucker N, Durham P J and Temmerman W M 1988 *Phys. Rev.* B **37** 123
[36] Wertheim G K, Guggenheim H J and Hüffner S 1973 *Phys. Rev. Lett.* **30** 1050
Eastman D E and Freeouf J F 1975 *Phys. Rev. Lett.* **34** 395
[37] Zaanen J and Sawatzky G A 1987 *Can. J. Phys.* **65** 1262
[38] Hirokawa K, Kadowaki H and Ubikoshi K 1985 *J. Phys. Soc. Japan* **54** 3526
[39] Kuiper P, Kruizinga G, Ghijsen J, Sawatzky G A and Verwey H 1989 *Phys. Rev. Lett.* **62** 221
[40] Bronger W, Bade H and Klemm W 1964 *Z. Anorg. (Allg.) Chem.* **333** 188
Goodenough J B, Wickham D G and Croff W J 1958 *J. Phys. Chem. Solids* **5** 17
[41] Korotin M A, Postnikov A V, Neumann T, Borstel G, Anisimov V I and Methfessel M 1994 *Phys. Rev.* B **49** 6548
[42] Okamoto H *et al* 1990 *Phys. Rev.* B **42** 10 381
[43] Anisimov V I, Albers R C, Wills J M, Allouani M and Wilkins J W 1995 *Phys. Rev.* B **52** R6975
[44] Anisimov V I, Korotin M A, Zaanen J and Andersen O K 1992 *Phys. Rev. Lett.* **68** 345
[45] Kugel K I and Khomskii D I 1982 *Usp. Fiz. Nauk.* **136** 621 (Engl. Transl. 1982 *Sov. Phys.–Usp.* **25** 231)
[46] Lichtenstein A I, Katsnelson M I, Antropov V P and Gubanov V A 1987 *J. Magn. Magn. Mater.* **67** 65
[47] Satija S K, Axe J D, Shirane G, Yoshizawa H and Hirokawa K 1980 *Phys. Rev.* B **21** 2001
Hutchings M T, Ikeda H and Milne J M 1979 *J. Phys. C: Solid State Phys.* **12** L739
[48] Zaanen J, Sawatzky G A and Allen J W 1985 *Phys. Rev. Lett.* **55** 418

[49] Weber W 1987 *Phys. Rev. Lett.* **58** 1371
[50] Zhang F C and Rice T M 1988 *Phys. Rev.* B **37** 3759
[51] Hybertsen M S *et al* 1990 *Phys. Rev.* B **41** 11 068
[52] Egami T *et al* 1991 *Electronic Structure and Mechanisms of High Temperature Superconductivity* ed J Ashkenazi and G Vezzoli (New York: Plenum)
[53] Anisimov V I, Ezhov S Yu, Elfimov I, Solovyev I V and Rice T M 1996 *Phys. Rev. Lett.* **76** 1735
[54] Korotin M A, Ezhov S Yu, Solovyev I V, Anisimov V I, Khomskii D I and Sawatzky G A 1996 *Phys. Rev.* B **54** 5309
[55] Foex G 1938 *J. Physique Radium* **9** 37
[56] Jaccarino V, Wertheim G K, Wernick J H, Walker L R and Arajs S 1987 *Phys. Rev.* **160** 476
[57] Takahashi Y and Moriya T 1979 *J. Phys. Soc. Japan* **46** 1451
Evangelou S N and Edwards D M 1983 *J. Phys. C: Solid State Phys.* **16** 2121
[58] Shirane G, Fisher J E, Endoh Y and Tajima K 1987 *Phys. Rev. Lett.* **59** 351
Tajima K, Endoh Y, Fisher J E and Shirane G 1988 *Phys. Rev.* B **38** 6954
[59] Mason T *et al* 1992 *Phys. Lett.* **69A** 490
Aeppli G 1994 *Strongly Correlated Electronic Materials* ed K S Bedell *et al* (New York: Addison-Wesley) p 3
[60] Mandrus D *et al* 1995 *Phys. Rev.* B **51** 4763
and see also
Sales B C *et al* 1994 *Phys. Rev.* B **50** 8207
and
Fu C and Doniach S 1995 *Phys. Rev.* B **51** 17 439
[61] Mattheiss L F and Hamann D R 1993 *Phys. Rev.* B **47** 13 114
[62] Raccah P M and Goodenough J B 1967 *Phys. Rev.* **155** 932
[63] Asai K, Yokokura O, Nishimori N, Chou H, Tranquada J M, Shirane G, Higuchi S, Okajima Y and Kohn K 1994 *Phys. Rev.* B **50** 3025
[64] Verwey E J W and Haayman P W 1941 *Physica* **8** 979
Verwey E J, Haayman P W and Romeijn F C 1947 *J. Chem. Phys.* **15** 181
[65] Fujii Y *et al* 1975 *Phys. Rev.* B **11** 2036
Izumi M and Shirane G 1975 *Solid State Commun.* **17** 433
Ida S *et al* 1978 *J. Appl. Phys.* **49** 1456
[66] Chainani A, Yokoya T, Morimoto T, Takahashi T and Todo S 1995 *Phys. Rev.* B **51** 17 976
Park J-H, Tjeng L, Allen J W, Metcalf P and Chen C T 1996 *Preprint*
[67] Yanase A and Saratory K 1984 *J. Phys. Soc. Japan* **53** 312
Zhang Z and Satpathy S 1991 *Phys. Rev.* B **44** 13 319
[68] Anisimov V I, Elfimov I S, Hamada N and Terakura K 1996 *Phys. Rev.* B **54** 4387
[69] Anisimov V I, Kuiper P and Nordgren J 1994 *Phys. Rev.* B **50** 8257
[70] Zaanen J 1986 *PhD Thesis* University of Groningen
[71] Anisimov V I, Antropov V P, Liechtenstein A I, Gubanov V A and Postnikov A V 1988 *Phys. Rev.* B **37** 5598
[72] Georges A, Kotliar G, Krauth W and Rosenberg M J 1996 *Rev. Mod. Phys.* **68** 13
[73] Bickers N E and Scalapino D J 1989 *Ann. Phys., NY* **193** 206
[74] Andersen O K, Jepsen O, Liechtenstein A I and Mazin I I 1994 *Phys. Rev.* B **49** 4145
[75] Ding H *et al* 1995 *Phys. Rev. Lett* **74** 2784